# Cholesterol-rich naked mole-rat brain lipid membranes are susceptible to amyloid beta-induced damage *in vitro*

Daniel Frankel[1], Matthew Davies[1], Bharat Bhushan[1], Yavuz Kulaberoglu[2], Paulina Urriola-Munoz[2], Justine Bertrand-Michel[3], Melissa R. Pergande[4], Andrew A. Smith[5], Swapan Preet[5], Thomas J. Park[6], Michele Vendruscolo[5], Kenneth S. Rankin[7], Stephanie M. Cologna[4], Janet R. Kumita[2,5], Nicolas Cenac[8], Ewan St John Smith[2]

[1]School of Engineering, Newcastle University, Newcastle Upon Tyne NE1 7RU, UK
[2]Department of Pharmacology, University of Cambridge, Cambridge, CB2 1PD, UK
[3]MetaToulLipidomics Facility, INSERM UMR1048, Toulouse, France
[4]Department of Chemistry, University of Illinois at Chicago, Chicago, IL 60607, USA
[5]Centre for Misfolding Diseases, Department of Chemistry, University of Cambridge, Cambridge, CB2 1EW, UK
[6]Department of Biological Sciences, University of Illinois at Chicago, Chicago, IL 60607, USA
[7]Translational and Clinical Research Institute, Newcastle University, Paul O'Gorman Building, Framlington Place, Newcastle upon Tyne, NE2 4HH, UK
[8]IRSD, INSERM, INRA, INP-ENVT, Toulouse University 3 Paul Sabatier, Toulouse, France

**Correspondence to:** Daniel Frankel, Nicolas Cenac, Ewan St John Smith; **email:** daniel.frankel@newcastle.ac.uk, Nicolas.cenac@inserm.fr, es336@cam.ac.uk
**Keywords:** Naked mole-rat, neurodegeneration, amyloid beta, brain, lipidomics
**Received:** August 3, 2020        **Accepted:** October 3, 2020        **Published:** November 4, 2020

## ABSTRACT

Naked mole-rats are extraordinarily long-lived rodents that offer unique opportunities to study the molecular origins of age-related neurodegenerative diseases. Remarkably, they do not accumulate amyloid plaques, even though their brains contain high concentrations of amyloid beta (Aβ) peptide from a young age. Therefore, they represent a particularly favourable organism to study the mechanisms of resistance against Aβ neurotoxicity. Here we examine the composition, phase behaviour, and Aβ interactions of naked mole-rat brain lipids. Relative to mouse, naked mole-rat brain lipids are rich in cholesterol and contain sphingomyelin in lower amounts and of shorter chain lengths. Proteins associated with the metabolism of ceramides, sphingomyelins and sphingosine-1-phosphate receptor 1 were also found to be decreased in naked mole-rat brain lysates. Correspondingly, we find that naked mole-rat brain lipid membranes exhibit a high degree of phase separation, with the liquid ordered phase extending to 80% of the supported lipid bilayer. These observations are consistent with the 'membrane pacemaker' hypothesis of ageing, according to which long-living species have lipid membranes particularly resistant to oxidative damage. We also found that exposure to Aβ disrupts naked mole-rat brain lipid membranes significantly, breaking the membrane into pieces while mouse brain derived lipids remain largely intact upon Aβ exposure.

## INTRODUCTION

The naked mole-rat (*Heterocephalus glaber*) is a long-lived species having a life span that can exceed 30 years [1, 2], which is nearly ten times longer than that of rodents of comparable size. Possessing many pedomorphic features [3, 4] and defying many of the signs of ageing [5], the naked mole-rat does not

appear to develop age-related neurodegenerative disease [6, 7].

Considering that Aβ is a pathogenic agent in AD [8], it was perhaps surprising that the naked mole-rat brain was observed to have high levels of Aβ, exceeding in particular those found in the commonly used 3×Tg transgenic mouse model of AD, even in the brains of young animals [6]. Although the exact role of Aβ in AD remains controversial [9], numerous drugs targeting Aβ pathways failing in clinical trials, amyloid plaques are a hallmark of the diseased brain. It is remarkable that no such amyloid plaques are found in naked mole-rat brains despite the high levels of Aβ [6]. Somehow, therefore, naked mole-rats appear to have a strong Aβ homeostasis system that enables them to live for years with this neurotoxic peptide. Thus, understanding why amyloid plaques do not form in naked mole-rat brains is of particular interest. This question is likely to have a complex answer as comparison of the human and naked mole-rat variants of Aβ shows only a single amino acid difference, which alters the aggregation kinetics, but not the degree of toxicity to mouse hippocampal neurons [6].

In this work we investigated whether the resistance to the neurotoxic effects of Aβ in the naked mole-rat can be traced back to specific properties of the lipid membranes of this animal, given that it is well established that lipid membranes can affect the aggregation of Aβ [10–13]. In particular, there is a strong link between cholesterol and AD, which could be related to its role in modulating the interaction between Aβ and lipid membranes [14–16]. Naked mole-rat lipids from brains and other tissues have been analysed in relation to their role in the membrane pacemaker theory of ageing, which states that long-lived species have membrane compositions that resist peroxidation, a proposed mechanism in resistance to ageing [17]. In naked mole-rat brains and within other tissues, it was observed that there was significantly less docosahexanoic acid (DHA), a fatty acid which is particularly susceptible to peroxidation, than that found in mice. In addition, it was reported that naked mole-rat membranes contain more vinyl ether linked phosphoplipids (plasmalogens) which are resistant to peroxidation [18, 19]. Plasmalogens are highly enriched in lipid rafts and contribute to their stability [20]. Thus, a high level of this ether lipid may be an indicator of a high raft content, or increased raft stability [21].

Here we used atomic force microscopy (AFM) to investigate the mechanical properties of lipid membranes as this method presents many advantages for examining lipid bilayer based systems, in particular its ability to quantify two dimensional ordering and to follow interactions between membrane and peptides in real time [22, 23]. More specifically, we combined AFM with lipidomics to compare naked mole-rat and mouse brain lipids in terms of composition and two dimensional ordering. We then used AFM to follow the interactions of synthetic human Aβ with brain-derived lipid membranes from both mouse and naked mole-rat. The membrane pacemaker theory of ageing suggests that cell membranes of long-lived species will possess more peroxidation resistant species which may also be raft forming [18]. We thus hypothesise that naked mole-rat brain derived lipid bilayers show a high degree of phase separation (two-dimensional ordering) and that there may be a unique lipid signature that protects the membranes against Aβ-induced damage.

## RESULTS

### Comparison of the lipid membrane compositions of naked mole-rat and mouse brains

Mass spectrometry of brain total lipid extract shows that there are key differences between naked mole-rat and mouse brain lipids, which may have implications for Aβ assembly and membrane interactions. Firstly, naked mole-rat brains have significantly more cholesterol than mouse brains (Figure 1A). Also of note is the relatively low level of sphingomyelin in naked mole-rat brains relative to mouse (Figure 1B). Although it has been reported that the levels of brain sphingomyelin positively correlate with Aβ plaques, other studies show the opposite correlation between sphingomyelin and AD [24]. In contrast to the observations for cholesterol and sphingomyelin, the concentrations of the total phospholipids and ceramides were not different between naked mole-rat and mouse brains (Figure 1C, 1D). The relative abundances of these different lipid species were evaluated and presented as heatmaps (Figure 1E, 1F) and as tables (Supplementary Tables 1–6).

We found that these lipidomic profiles were different between mouse and naked mole-rat brains, as illustrated by a clustering of mouse and naked mole-rat depending on the number of carbon atoms of the phospholipids, or of sphingomyelins and ceramides (Figure 1E, 1F, top dendrograms). Concerning the phospholipids, four major groups of lipids were identified: cluster 1 contained lipids which were more abundant in naked mole-rat than mouse brains, clusters 2 and 3 contained lipids which were not differentially expressed between mouse and naked mole-rat brains, and cluster 4 contained lipids that were more abundant in mouse brains (Figure 1E). However, these four clusters did not reveal a distinct pattern of species. The ceramide and sphingolipid clustering highlighted 4 clusters: cluster 1 was composed of lipids more abundant in mouse brains, cluster 3 by lipids more abundant in naked mole-rat
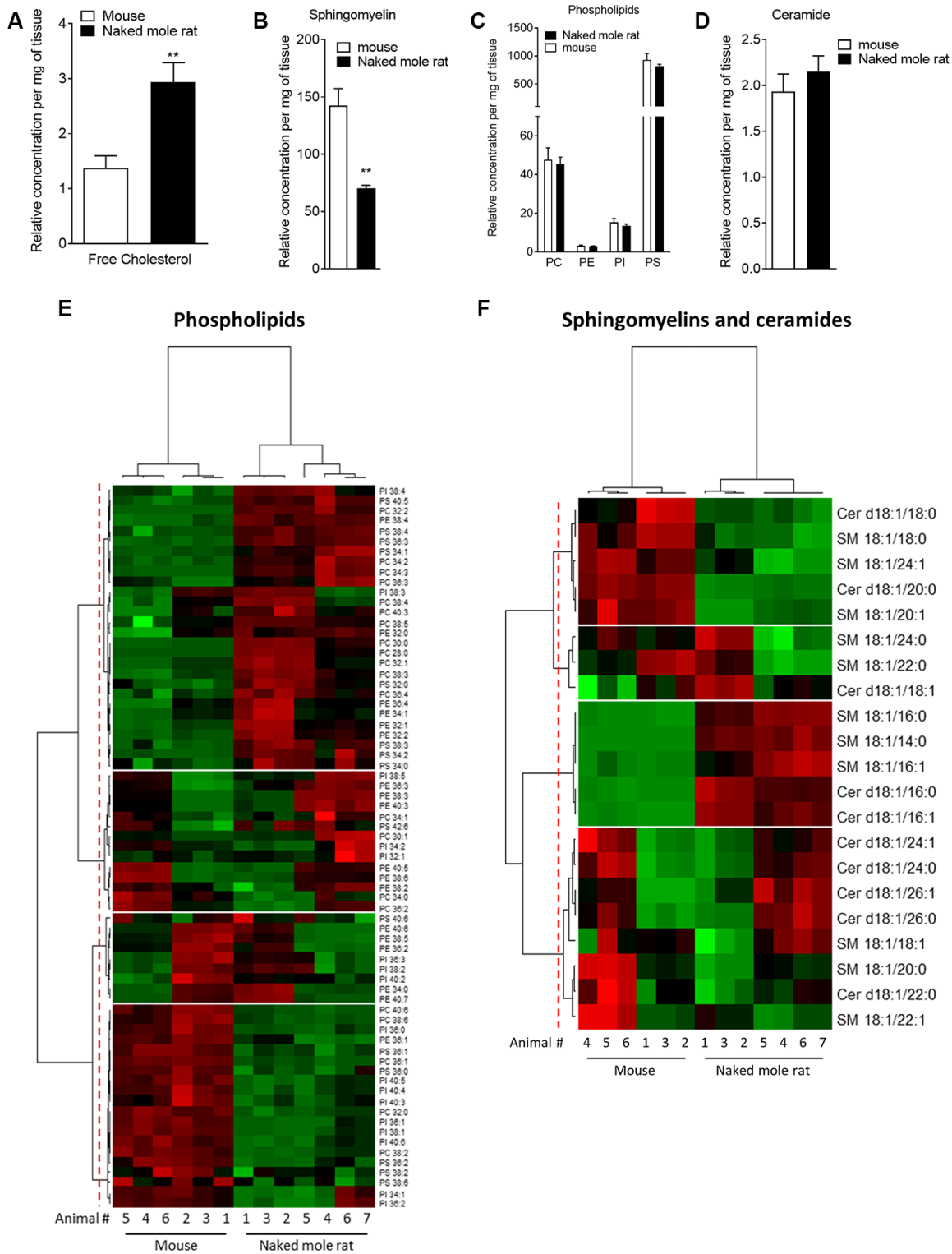
**Figure 1. Mass spectrometry of brain derived total lipid extract.** (**A–D**) Quantification of cholesterol (**A**), sphingomyelin (**B**), phosphatidylcholine (PC), phosphatidylethanolamine (PE), phosphatidylinositol (PI) and phosphatidylserine (PS) (**C**), and ceramides (**D**) in lipid extract from mouse (white bar) or naked mole-rat (black bar) brains. Data are expressed as mean ± SEM. Statistical analysis was performed using the Mann-Whitney test. **p<0.01, significantly different from mouse group. Lipids were extracted from the brains of 7 naked mole-rats and 6 mice (2 independent experiments). (**E**) Heat map of the different phospholipids quantified by LC-MS/MS. Data are shown in a matrix format: each row represents a single phospholipid, and each column represents the lipid extract of the brain of one animal (6 mice and 7 naked mole-rat). Each colour patch represents the normalized quantity of phospholipid (row) in a single animal brain (column), with a continuum of quantity from bright green (lowest) to bright red (highest). The pattern and length of the branches in the left

dendrogram reflect the relatedness of the phospholipids. The dashed red line is the dendrogram distance used to cluster the phospholipids. The pattern and length of the branches in the top dendrogram reflect the relatedness of the different animals. (**F**) Heat map of the different sphingomyelins and ceramides quantified by LC-MS/MS. Data are shown in a matrix format: each row represents a single sphingomyelin or ceramide, and each column represents the lipid extract of the brain of one animal (6 mice and 7 naked mole-rat). Each colour patch represents the normalized quantity of sphingomyelin or ceramide (row) in a single animal brain (column), with a continuum of quantity from bright green (lowest) to bright red (highest). The pattern and length of the branches in the left dendrogram reflect the relatedness of the sphingomyelins and ceramides. The dashed red line is the dendrogram distance used to cluster the phospholipids. The pattern and length of the branches in the top dendrogram reflect the relatedness of the different animals.

brains, and clusters 2 and 4 being no different between the two species. Interestingly, sphingomyelin and ceramides preferentially presented in naked mole-rat brains (cluster 3) were the shortest lipids quantified. Thus, this lipid analysis revealed differences in the lipid composition of mouse and naked mole-rat brains.

With the finding that multiple lipids were present at different levels in the two species, we sought to investigate if these differences extended at the protein level. Using an untargeted differential proteomic study, we compared protein abundance between mice and naked mole-rats (Figure 2). We observed decreased levels of acid ceramidase, the enzyme responsible for ceramide degradation into sphingosine – a primary constituent of sphingolipids – and free fatty acids, in naked mole-rat cerebellar tissue (Figure 2A). Ceramide synthase 2, which catalyses the formation of ceramide with selectivity towards very long, C22:0 – C24:0 chains, was also decreased in naked mole-rats in both hippocampal and cerebellar tissue lysates (Figure 2B, 2C). Sphingomyelinase (sphingomyelin phosphodiesterase 3 / neutral sphingomyelinase 2), which catalyses the hydrolysis of sphingomyelin to ceramide and phosphocholine, was also decreased in naked mole-rat hippocampal tissue (Figure 2D) as was sphingosine-1-phosphate receptor 1 in the cerebellum and cerebral cortex (Figure 2E, 2F). The normalized protein abundances are provided for each brain region in the supplemental information (Supplementary Figure 1). Due to the complexities of sphingomyelin biosynthesis and degradation, the proteomic changes observed could align with the lower sphingomyelin levels observed. For example, lower acid ceramidase abundance results in less sphingosine generation by ceramide cleavage, and one pathway for sphingomyelin production involves sphingosine conversion to sphingosyl-phosphocholine and then into sphingomyelin. Overall, naked mole-rat brain lipids contained a higher concentration of cholesterol and lower concentration of sphingomyelins, which were of shorter length than those present in mouse brains, but contained a higher percentage of saturated sphingomyelin (Supplementary Figure 2). We completed the comparison of lipid composition of naked mole-rat and mouse brains by quantifying the concentration in total fatty acids (FA). No significant differences were

observed between the concentrations of saturated (SFA), monounsaturated (MUFA) and polyunsaturated fatty acids (PUFA) in mouse and naked mole-rat brains (Figure 3A–3C). However, the n-6/n-3 ratio of PUFAs was increased in naked mole-rat brains compared to mouse brains (Figure 3D). The relative abundances of these FA were evaluated and presented as a heatmap (Figure 3E) and as a table (Supplementary Table 7). We found that the FA profile was different between mouse and naked mole-rat brains, as illustrated by a clustering of mouse and naked mole-rat depending on the number of carbon atoms within the FA (Figure 3E). Three major groups of FA were identified: cluster 1 contained lipids which were more abundant in mouse brains, cluster 2 contained FA which were not differentially expressed between mouse and naked mole-rat brains, and cluster 3 contained lipids that were more abundant in naked mole-rat brains (Figure 3E). As observed for the ceramides and sphingomyelin, the SFA and MUFA abundant in naked mole-rat brains (cluster 3) were of shorter length than those present in mouse brains. Supplementary Tables 1–7 provide a detailed comparative overview of the percentage of different lipid species identified in mouse and naked mole-rat brain lipids.

## Aβ avoids gel phase domains in model lipid membranes

Prior to an AFM examination of the interactions between human Aβ and the brain tissue derived lipids, we used a simple model system comprising of just two lipids, DOPC and DPPC. This system exhibits phase separation and provides a well-defined comparison for the more complex mixture of lipids present in brain derived lipids. When the binary system was mixed in a molar ratio of 3:1 of DOPC-to-DPPC, we observed the classic phase-separated DPPC gel domains surrounded by the liquid disordered DOPC (Figure 4A). The origin of the islands of DPPC is due to the packing arrangement of DPPC chains, resulting in a height difference of around 1.5 nm to the surrounding DOPC (Figure 4B). Such spontaneous phase separation behaviour in model systems has been used as a rationale for the existence of lipid rafts in cells [25]. After a 2-hour exposure to 8 μM of human Aβ the bilayer remained completely intact, but with

clearly visible features due to the Aβ peptide in between the DPPC gel phase domains, which are absorbed on top of the DOPC liquid disordered phase (highlighted by blue circle in Figure 4C). Upon closer inspection, the Aβ was observed to avoid the gel phase domains, such that the central DPPC gel domain was surrounded, but not covered, by the peptide (Figure 4D).
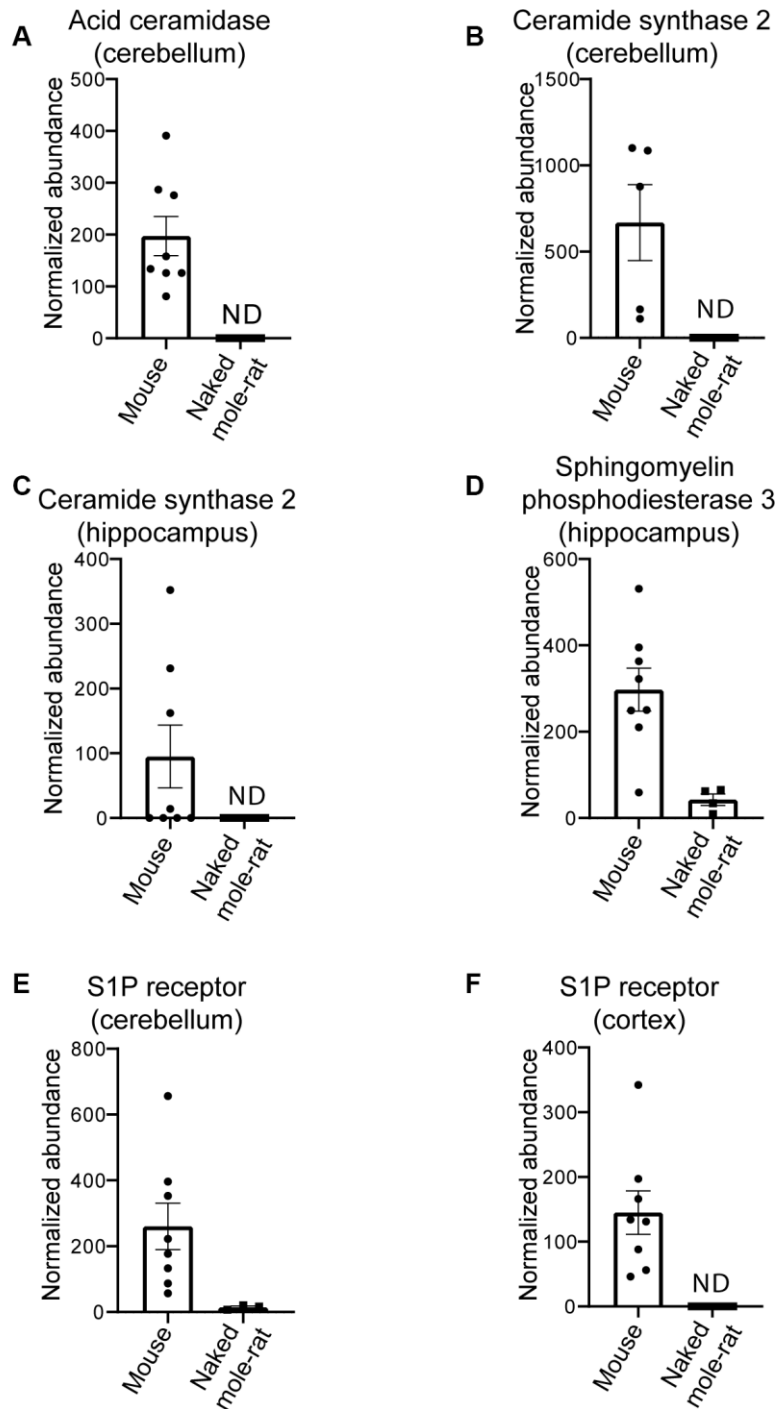


**Figure 2. Differential proteins in mouse compared to naked mole-rats.** (**A**) Differential levels of acid ceramidase in cerebellar tissue. Ceramide synthase 2 is decreased in naked mole-rat tissues in both the cerebellum (**B**) and hippocampus (**C**). Sphingosine phosphodiesterase 3, a member of the sphingomyelinase family (also called neutral sphingomyelinase 2) is decreased in naked mole-rat hippocampus (**D**) where sphingosine-1-phosphate receptor 1 is decreased in the cerebellum (**E**) and the cerebral cortex (**F**). ND indicates not detected or quantifiable. The homology between the two species, relative to mouse, was 81% (**A**), 90% (**B**), 91.3% (**C**) and 95% (**D**).

## Lipid bilayers formed from naked mole-rat brain-derived total lipid extracts exhibit a high degree of phase separation

Lipid bilayers formed from naked mole-rat brain-derived total lipid extracts were formed on a cleaved mica surface and were found to exhibit a high degree of phase separation, with the characteristic islands (Figure 5A). These islands could occupy an area greater than 80% of that of the whole lipid membrane. At higher magnification, it was sometimes possible to distinguish a two-tier raft (Figure 5B, 5C), but this was not seen in all preparations. However, the high degree of phase separation was observed in lipids extracted from all naked mole-rat brains studied. For comparison, mouse brain lipids exhibited little to no phase separation, such that a lipid membrane formed with little to no deviation in height and structure (Figure 5D).

By indenting the conical AFM tip into the lipid bilayer it is possible to measure the breakthrough force [26], which is the force required to push through the soft thin film (Figure 6A, 6B), thereby providing an indication of the membrane fluidity. It also allows the measurement of membrane thickness, which is a necessary confirmation that a thin soft bilayer is being imaged. Although no difference was observed in the thickness of lipid bilayer membranes formed from mouse or naked mole-rat brain derived lipids (Figure 6C), the breakthrough force measurements for naked mole-rat membranes were significantly higher than mouse (Figure 6D), meaning that naked mole-rat lipid bilayer membranes are stiffer. The enhanced stiffness of naked mole-rat lipid bilayer membranes is most likely due to the increased cholesterol, which is known to increase membrane rigidity [27].

## Aβ disrupts lipid bilayers formed from naked mole-rat brain-derived total lipid extracts

Prior to exposure to Aβ, the mouse brain derived lipid bilayer had a characteristic morphology exhibiting almost no phase separation with only the occasional, small domain being visible (Figure 7A). When exposed
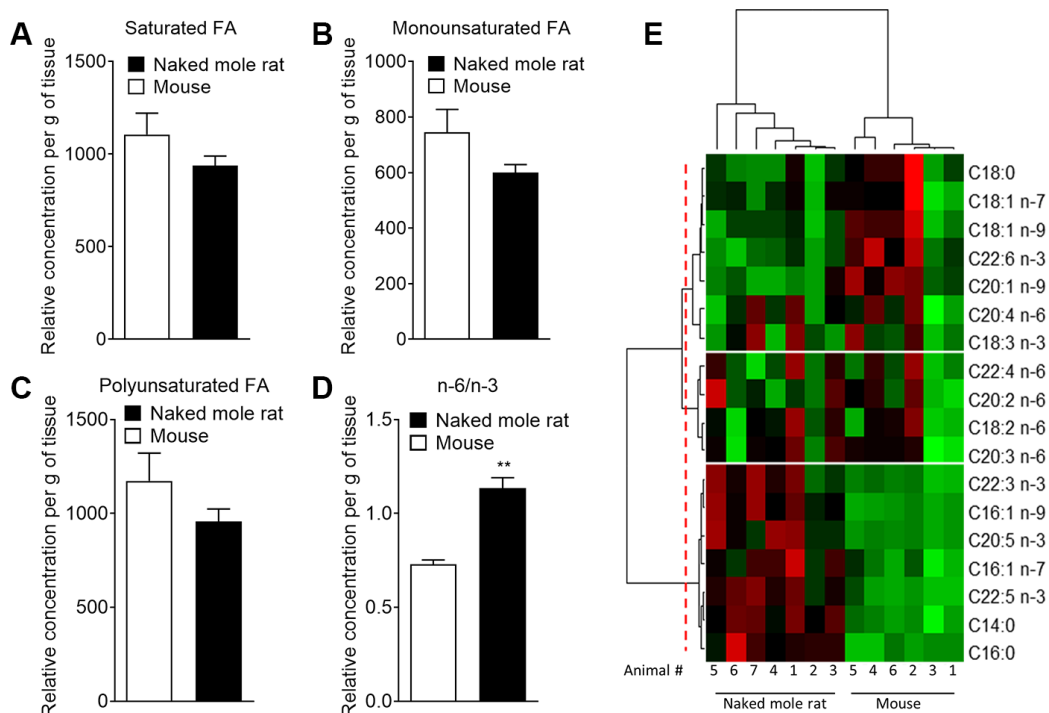


**Figure 3. Mass spectrometry of brain derived total fatty acids**. Lipids were taken from the brains of 7 naked mole-rats and 6 mice (2 independent experiments). Quantification of (**A**) saturated fatty acids, (**B**) monounsaturated fatty acids, (**C**) polyunsaturated fatty acids (PUFA), and (**D**) n-6 PUFA/n-3 PUFA ratio extract from mouse (white bar) or naked mole-rat (black bar) brains. Data are expressed as mean ± SEM. Statistical analysis was performed using Mann-Whitney test. **p<0.01, significantly different from mouse group. (**E**) Heat map of the different fatty acids (FA) quantified by LC-MS/MS. Data are shown in a matrix format: each row represents a single FA, and each column represents the lipid extract of the brain of one animal (6 mice and 7 naked mole-rat). Each colour patch represents the normalized quantity of FA (row) in a single animal brain (column), with a continuum of quantity from bright green (lowest) to bright red (highest). The pattern and length of the branches in the left dendrogram reflect the relatedness of the FA. The dashed red line is the dendrogram distance used to cluster the FA. The pattern and length of the branches in the top dendrogram reflect the relatedness of the different animals.

to 8 μM human Aβ for 2 hours, pores appeared in the mouse derived lipid bilayer (Figure 7B). The pores were not circular, and there was little sign of the Aβ that had caused them. A likely explanation is that the Aβ peptides sunk into the membrane because the height profile through the pores shows that they were less deep than the thickness of the bilayer (Figure 7C, 7D). It is important to note that the integrity of the membrane, as a whole, was maintained.

At variance with what was observed with mouse lipid bilayers, upon exposure of naked mole-rat lipid bilayers to human Aβ under the same conditions (8 μM for 2 hours), the naked mole-rat lipid bilayer membrane was disrupted (Figure 8). In contrast to the raft covered membrane observed under control conditions (Figure 8A), incubation with Aβ results in the presence of only fragments of lipid bilayer (Figure 8B, 8C), > 5 nm in height relative to the surface (consistent with the thickness of the bilayer rather than the height of a raft, Figure 8D). Membrane fragments after Aβ exposure were observed with lipid bilayers formed from lipids extracted from all 3 brains examined.

## DISCUSSION

Our lipidomic data show fatty acid and phospholipid trends between mouse and naked mole-rat that are
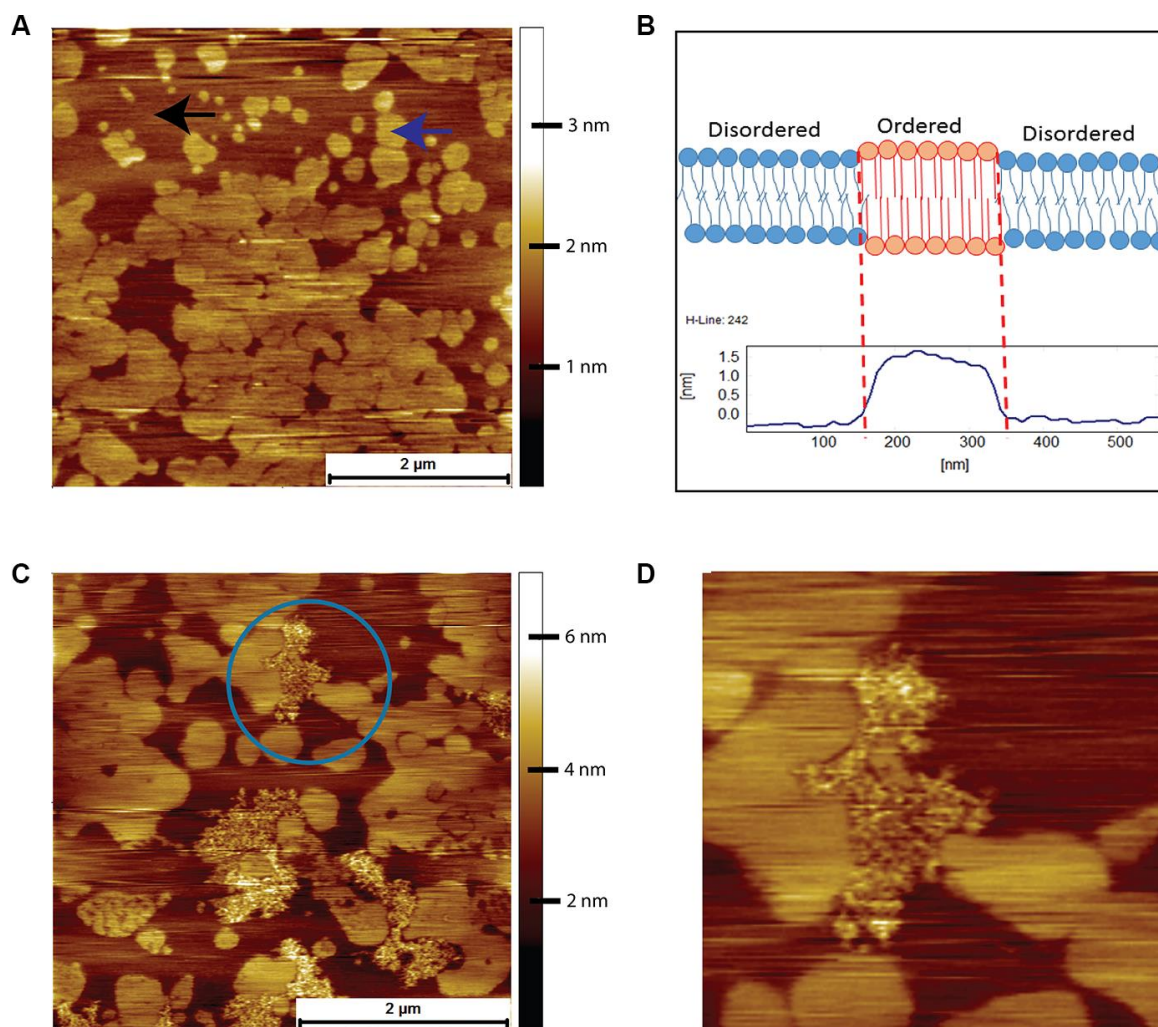


**Figure 4. AFM contact mode images in PBS of DOPC/DPPC model supported lipid bilayers and their interactions with human Aβ peptide.** (**A**) Supported bilayer made from DOPC to DPPC in a molar ratio of 3:1. Typical phase separation is observed with the DPPC gel phase islands (example indicated by the blue arrow) surrounded by the liquid disordered DOPC phase (example indicated by the black arrow). (**B**) Proposed origin of height difference of the gel phase relative to liquid disordered phase. (**C**) DOPC/DPPC bilayer after exposure for 2 hours to 8 μM of human Aβ. The Aβ has adsorbed exclusively onto the DOPC liquid disordered phase, the DPPC gel phase remaining untouched. (**D**) A zoom in of the area enclosed in the circle in (**C**)., the Aβ being seen to avoid the DPPC gel domains, even the small central DPPC gel domain remaining untouched.

consistent with the previous work of Mitchell et al. [19]. However, in addition we found that cholesterol levels in naked mole-rat brains are significantly higher than in mouse brains and that sphingomyelin levels are significantly lower. Moreover, in naked mole-rats, the sphingomyelin measured has a shorter length and less fatty acid chain unsaturation compared to that of mouse. These differences play an important role for phase separation, as sphingomyelin containing shorter and saturated fatty acid chains forms more readily close-packed and highly ordered bilayers [28]. In addition, lipid oxidation which has been implicated in several

pathological process, including neurodegenerative diseases [29], starts by the transformation of lipid molecules with double bonds such as unsaturated fatty acids to lipid hydroperoxides via the free radical mechanism [30]. Thus, with a lower degree of unsaturation in the fatty acid chain of naked mole-rat brain sphingomyelin coupled to a significant decrease in DHA concentration, the naked mole-rat should be less sensitive to lipid oxidation than mouse.

These lipid findings are supported by proteomic analysis of brain lysates showing that critical lipid
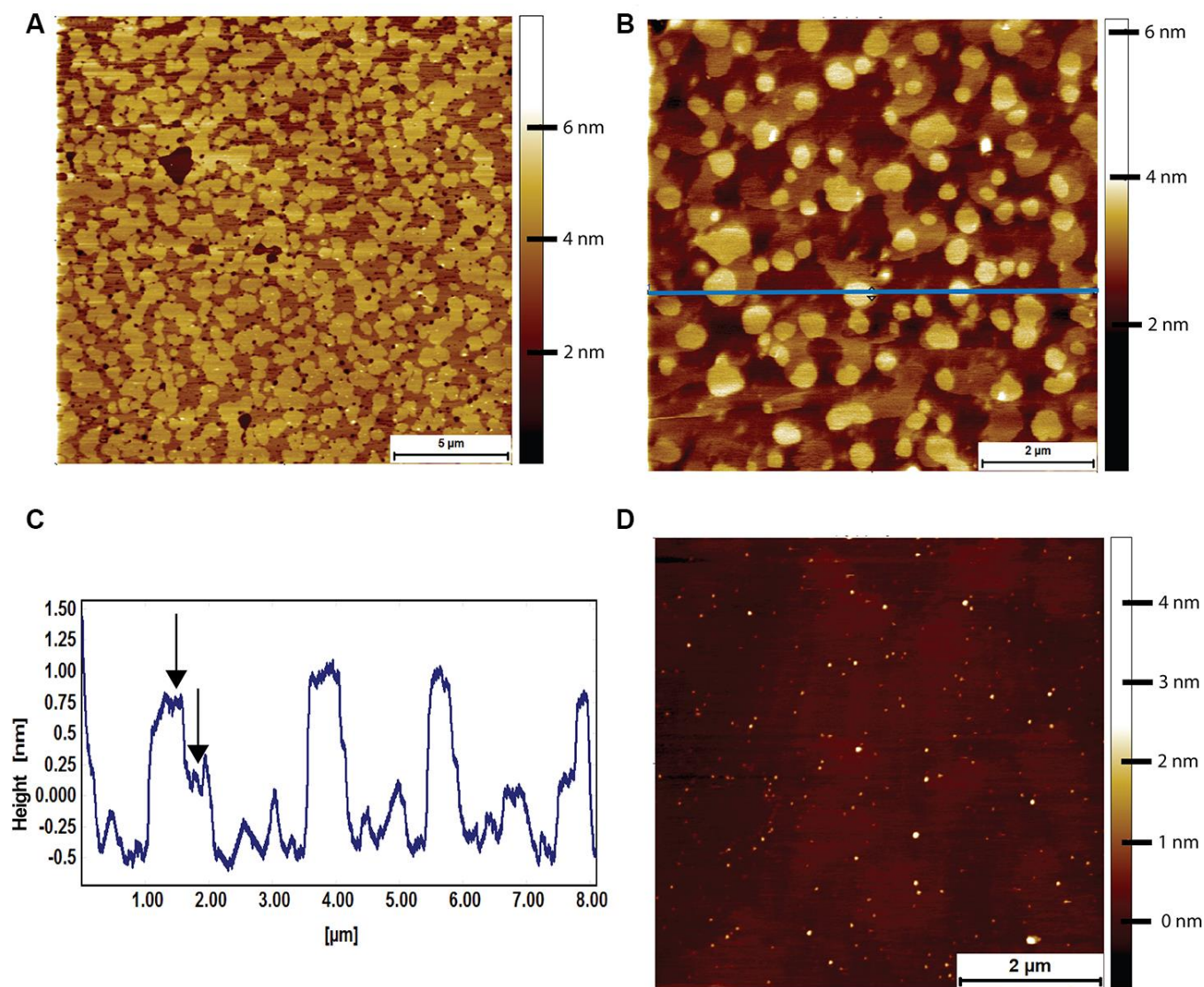


**Figure 5. AFM tapping mode images of brain-derived supported lipid bilayers.** (**A**) Supported bilayer made from naked mole-rat brain-derived lipids in PBS. More than 80% of the membrane is made up of phase separated islands of ~1.5 nm in height relative to the surrounding liquid disordered phase. (**B**, **C**) Supported bilayer made of naked mole-rat brain lipids showing a two-tier raft structure, the horizontal blue line corresponding to the height profile in C, where the two-tier raft structure is evident from the peaks having a shoulder, the first at ~0.75 nm, the second at ~1.25 nm, indicated by arrows in the figure. (**D**) Supported lipid bilayer made from mouse brain derived lipids. In contrast to the naked mole-rat bilayers there is little evidence of phase separation.

metabolism enzymes were also altered in naked mole-rats compared to mice. For example, decreased ceramide synthase 2 levels in naked mole-rat brains may account for the high levels of short chain ceramides in naked mole-rat compared to mouse due to ceramide synthase 2 being responsible for generation of very long chain ceramides. Using AFM, we found that naked mole-rat brain lipids have a high level of phase separation, which is consistent with predictions from the membrane pacemaker theory. Regardless of whether such domains exist in a living cell, the lipids that are able to phase separate could have a role in protection against ageing. Mechanical measurements show that the extra cholesterol results in a stiffer membrane, but surprisingly, these phase-separated and stiffer membranes offer limited

protection against Aβ-induced damage. The susceptibility of naked mole-rat membranes to Aβ-induced damage was unexpected given the Aβ rich environment of the naked mole-rat brains and the lack of overt neurodegeneration in this species [6].

High serum cholesterol levels in middle-aged humans have been linked to higher risk of developing AD [31]. In addition, cholesterol in model membranes has been found to catalyse Aβ aggregation [16]. If these higher cholesterol levels in serum translate into higher cholesterol levels in neuron cell membranes, then it could be that higher Aβ aggregation and toxicity follow, hence an increased risk of AD. This possibility is consistent with the naked mole-rat data
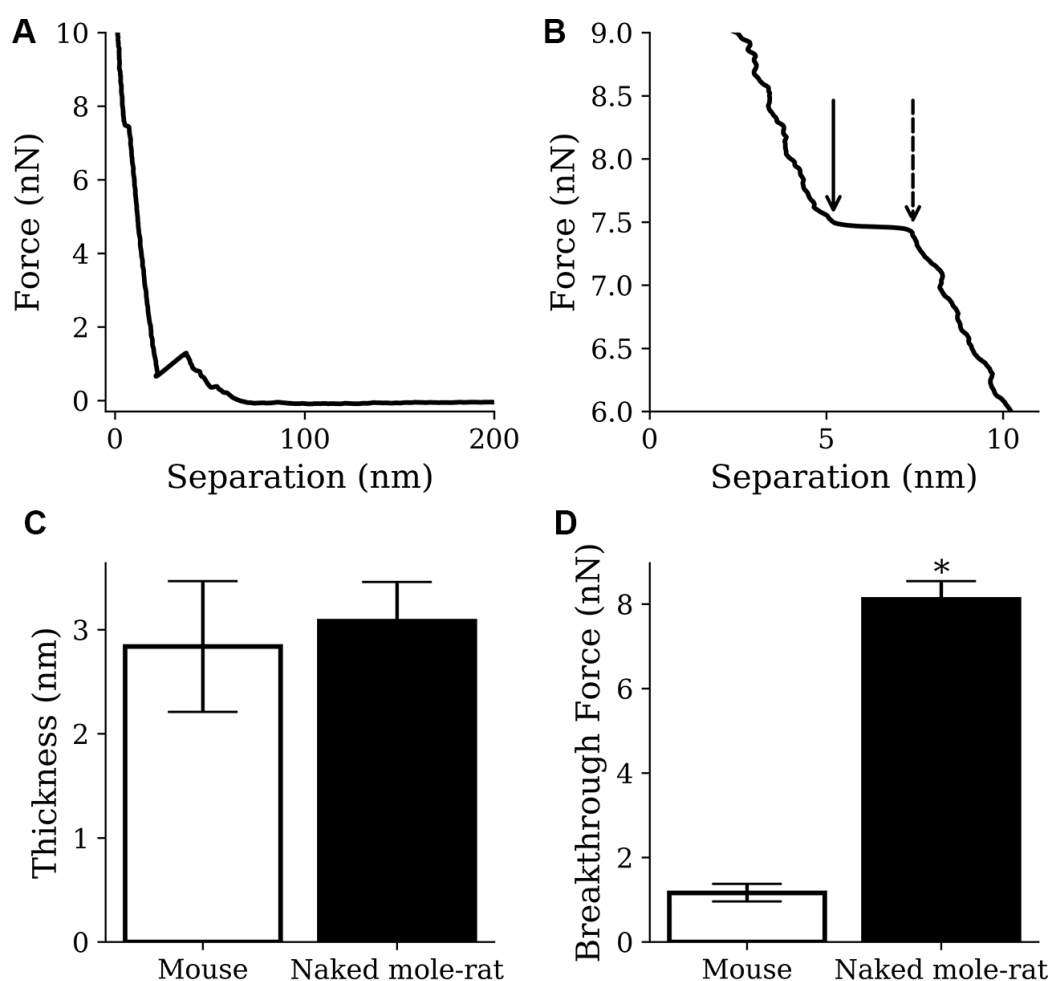


**Figure 6. AFM results from mouse samples (n=1220) and naked mole-rat samples (n=2859) lipid bilayer indentations.** (**A**, **B**) Example indentation on a naked mole-rat bilayer (A), where multiple breakthrough events were detected only the event closest to the mica (**B**) was recorded. The points indicated by the dashed and solid arrow in panel B show the start and end of the breakthrough event respectively. Thickness was recorded as the difference in separation between the points and breakthrough force was recorded at the start of the breakthrough indicated by the dashed arrow. (**C**) Thickness values of 3.1 ± 0.4 nm and 2.8 ± 0.6 nm were recorded for the naked mole-rat and mouse lipid bilayers respectively. (**D**) Breakthrough force values of 8.1 ± 0.4 nN and 1.2 ± 0.2 nN were recorded for the naked mole-rat and mouse lipid bilayers respectively. Data are expressed as mean ± SEM. Statistical analysis was performed using the unpaired t test. *p<0.05, significantly different from mouse group.

in that high cholesterol levels correspond to a high level of Aβ-induced membrane damage. However, considering the high levels of Aβ in naked mole-rat brains and the absence of obvious neurodegeneration, other, as yet unknown, neuroprotective mechanisms must exist.

Cell membranes consist of more than just phospholipids, with cytoskeleton, proteins and carbohydrates all contributing to membrane stability. Thus, the relative difference in composition and mechanical properties between mouse and naked mole-rat lipids

bilayers could be a significant contributor to the Aβ response in each species. It should also be noted that the total lipid extract from brain tissue includes not just lipids from cell membranes, but also from mitochondria and other organelles. Interestingly, the same susceptibility of naked mole-rat membrane lipids to damage was found when using naked mole-rat Aβ peptide (Supplementary Figures 3–6). This finding is despite the single amino acid difference in sequence, whereby histidine is replaced by arginine in naked mole rat Aβ. We also found that naked mole-rat Aβ readily forms fibres and fibrils (Supplementary Figures 3, 4)
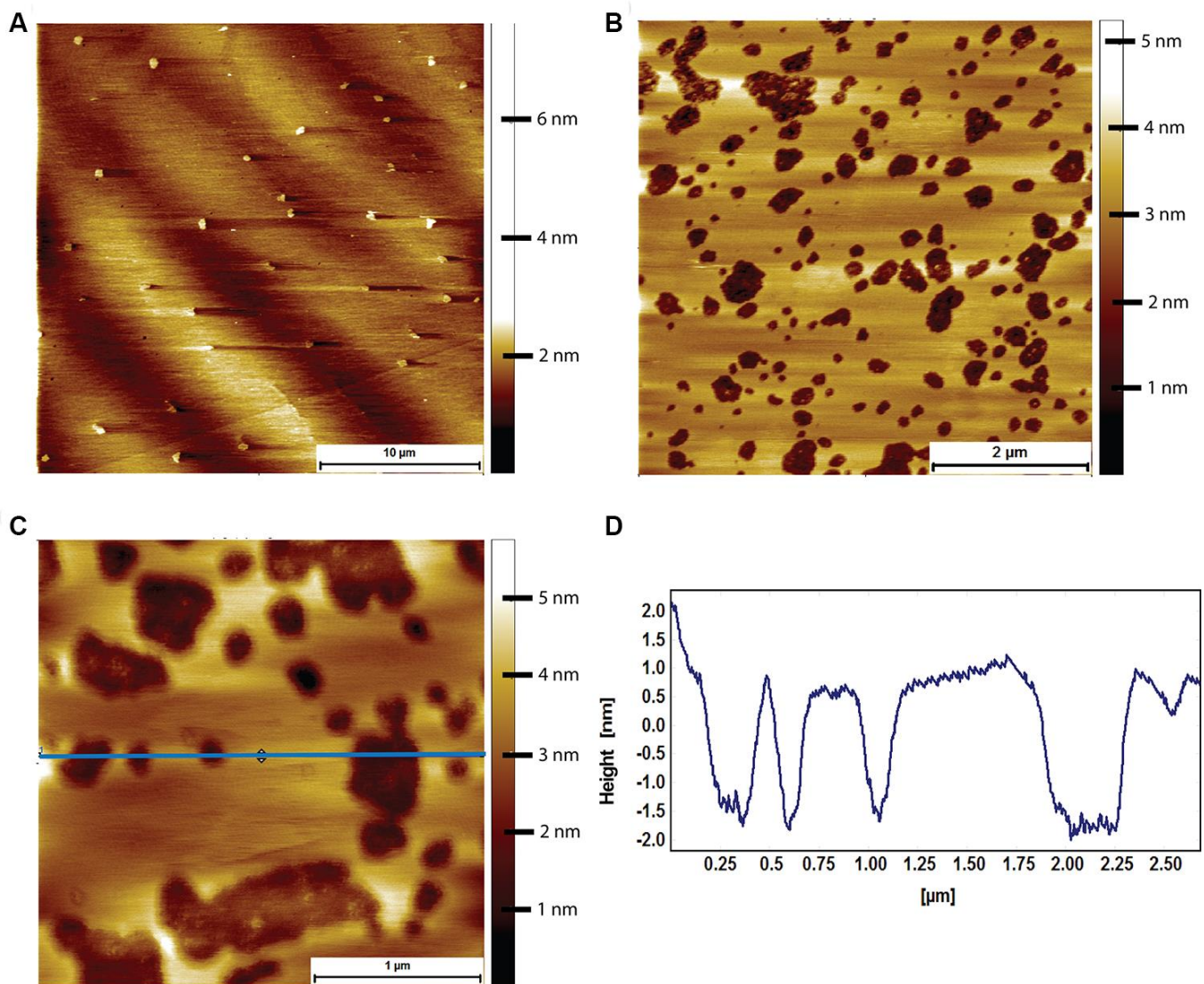


**Figure 7. AFM tapping mode images of mouse brain tissue derived supported lipid bilayers in PBS exposed to 8 μM of human Aβ for 2 hours.** (**A**) Large scale image showing a sparse amount of phase separation prior to Aβ adsorption. (**B**) Mouse brain derived lipid bilayer after exposure for 2 hours to 8 μM of human Aβ. Pits appear in the membrane, with some structure visible within the pits. (**C**) A close up of the pits showing that they do not break through the entire bilayer, i.e. they are not holes. (**D**) Line profile corresponding to the horizontal blue line in (**C**). The pits are between 2 and 2.5 nm deep, too shallow to be holes in the bilayer, which is ~3.1 nm thick.

as is the case with human Aβ. Again with mouse brain lipids, the naked mole-rat Aβ sinks into the bilayer, leaving the bilayer intact, but with holes (Supplementary Figure 5). Upon exposure to naked mole-rat Aβ, the naked mole-rat brain derived supported bilayers are broken up into membrane fragments (Supplementary Figure 6). This consistency in behaviour between human and naked mole-rat Aβ with respect to membrane interactions further demonstrates that mechanical lipid membrane properties alone are unlikely responsible for the absence of Abeta-induced neurodegeneration in naked mole-rats.

In summary we found that naked mole-rat brain lipids have high cholesterol and low sphingomyelin levels compared to mouse brain lipids, and that the bilayers formed from naked mole-rat brain lipids are unusual in terms of their high degree of phase separation. By contrast, both mouse (this paper) and pig [32] brain lipids show little or no sign of such two dimensional ordering. The comparative sensitivity of naked mole-rat lipid bilayers to Aβ-induced damage suggests that the naked mole-rats might have evolved neuroprotective mechanisms based more on resistance to oxidative processes than mechanical resistance
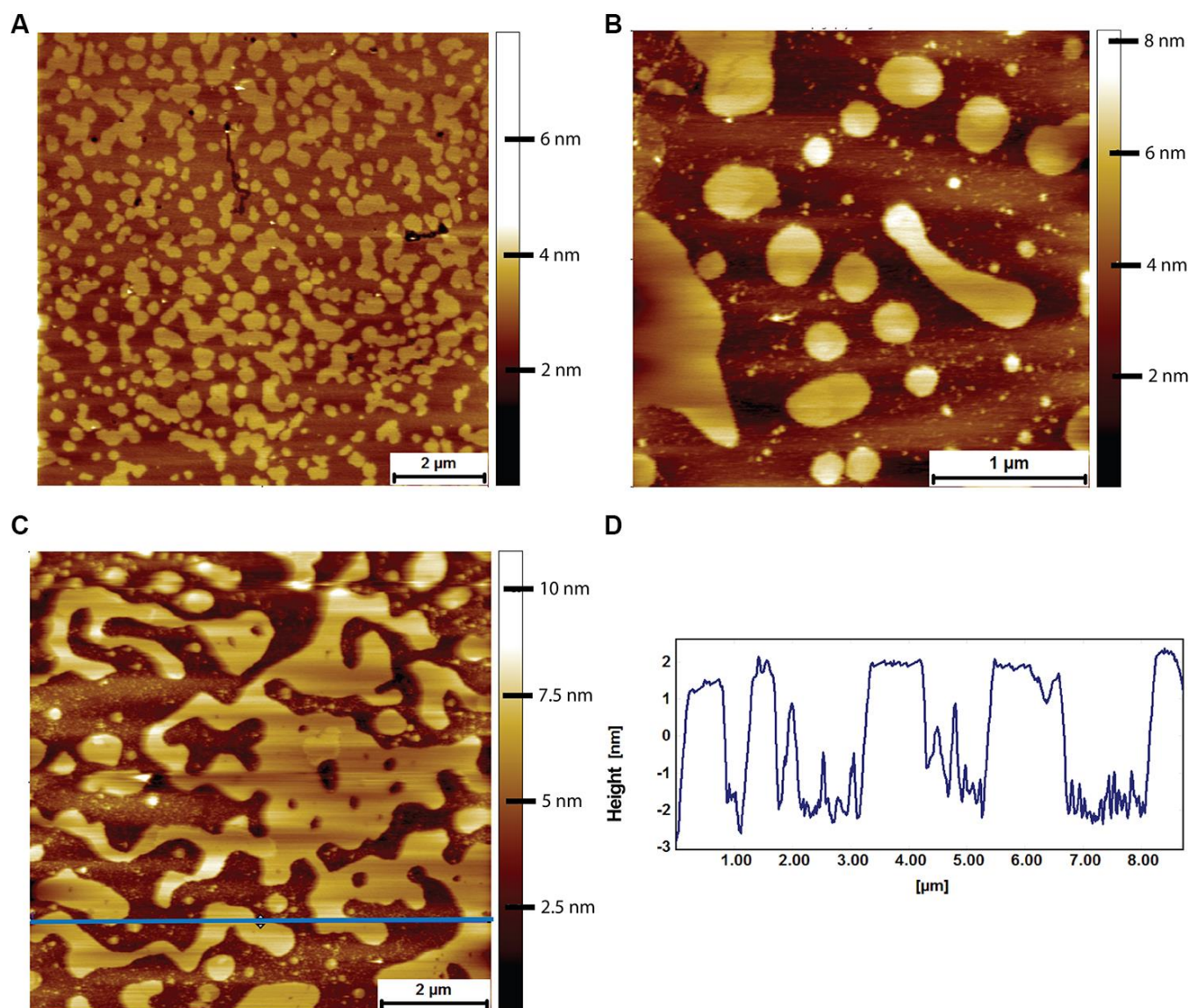


**Figure 8. AFM tapping mode images of naked mole-rat brain derived lipid bilayers exposed to 8 μM of human Aβ for 2 hours.** (**A**) The naked mole-rat brain derived bilayer before Aβ adsorption in PBS exhibiting the high degree of phase separation characteristic of naked mole-rat bilayers. (**B**, **C**) Naked mole-rat brain derived bilayer exposed to 8 μM of human Aβ for 2 hours. (**D**) A height profile corresponding to the blue horizontal line in (**C**), confirming the height of fragments to be of bilayer thickness of 4 nm.

to support a healthy brain within an Aβ-rich environment.

## MATERIALS AND METHODS

### Animals

Experiments were performed on lipids and proteins extracted from C57BL6/J mice and non-breeding naked mole-rats. A mixture of males and females were used of both species, all adults for lipid studies. For proteomic studies, mice (N=8) were euthanized at 2-weeks (N=4) and 6 months (N=4) of age. Similarly, NMRs were euthanized at 2-4 months (N=4) and 3 years (N=4) of age. Cerebellum, cortex and hippocampus were collected and flash frozen, as previously described [33]. Mice were conventionally housed with nesting material and a red plastic shelter in temperature-controlled rooms at 21° C, with a 12 h light/dark cycle and access to food and water *ad libitum*. Naked mole-rats were bred in-house and maintained in an inter-connected network of cages in a humidified (~55 %) temperature-controlled room at 28° C, with red lighting (08:00-16:00) and had access to food *ad libitum*. In addition, a heat cable provided extra warmth under 2-3 cages/colony. Mice were humanely killed by cervical dislocation of the neck and cessation of circulation, whereas naked mole-rats were killed by $CO_2$ exposure followed by decapitation. Experiments were conducted under the Animals (Scientific Procedures) Act 1986 Amendment Regulations 2012 under a Project License (P7EBFC1B1) granted to E. St. J. Smith by the Home Office and approved by the University of Cambridge Animal Welfare Ethical Review Body. Experiments performed for proteomic analysis were done so in accordance with institutionally-approved protocols at the University of Illinois at Chicago (PI – T.J. Park).

### Lipid extraction

Lipid extraction was performed according to a modified chloroform/methanol (2:1, v/v) procedure [34]. Briefly, frozen brain tissue from naked mole-rat or mouse was crushed into small pieces by razor in a petri dish, then the sample was transferred into a 15 mL tube and 2 mL of chloroform/methanol (2:1, v/v) was added; chloroform (Sigma 288306-1L), methanol (Fisher 10675112). The suspension was vortexed and incubated at room temperature with agitation for 20 min. After the incubation, 400 µL of 0.9% NaCl was added to the mixture and was then vortexed and centrifuged at 500 x g for 10 min to separate the organic phase from the aqueous phase. The chloroform (lower) layer was transferred into a new 1.5 mL tube and was centrifuged at 500 x g for 10 min. Finally, the supernatant was collected without touching the pellet and was transferred into a new 1.5 mL tube. The sample was stored at -80° C until the analysis.

### Brain neutral lipids analysis

Internal standards: glyceryl trinonadecanoate, stigmasterol, and cholesteryl heptadecanoate (Sigma) were added to 45 µL of lipid extract. Triglycerides, cholesterol, and cholesterol esters were analysed with gas-liquid chromatography on a Focus Thermo Electron system equipped with a Zebron-1 Phenomenex fused-silica capillary column (5 m, 0.25 mm i.d., 0.25 mm film thickness). Oven temperature was programmed to increase from 200 to 350° C at 5° C/min, and the carrier gas was hydrogen (0.5 bar). Injector and detector temperatures were 315° C and 345° C, respectively.

### Brain phospholipid, ceramide and sphingolipid analysis

Internal standards (Cer d18:1/15:0, 16 ng; PE 12:0/12:0, 180 ng; PC 13:0/13:0, 16 ng; SM d18:1/12:0, 16 ng; PI 16:0/17:0, 30 ng; PS 12:0/12:0, 156.25 ng; all from Avanti Polar Lipids) were added to 45 µL of lipid extract. Sample solutions were analysed using an Agilent 1290 UPLC system coupled to a G6460 triple quadripole spectrometer (Agilent Technologies). MassHunter software was used for data acquisition and analysis. A Kinetex HILIC column (Phenomenex, 50 × 4.6 mm, 2.6 µm) was used for LC separations. The column temperature was maintained at 40° C. Mobile phase A was acetonitrile and B was 10 mM ammonium formate in water at pH 3.2. The gradient was as follows: from 10% to 30% B in 10 min, 100% B from 10 to 12 min, and then back to 10% B at 13 min for 1 min to re-equilibrate prior to the next injection. The flow rate of the mobile phase was 0.3 ml/min, and the injection volume was 5 µl. An electrospray source was employed in positive (for Cer, PE, PC, and SM analysis) or negative ion mode (for PI and PS analysis). The collision gas was nitrogen. Needle voltage was set at +4000 V. Several scan modes were used. First, to obtain the naturally different masses of different species, we analysed cell lipid extracts with a precursor ion scan at 184 m/z, 241 m/z, and 264 m/z for PC/SM, PI, and Cer, respectively. We performed a neutral loss scan at 141 and 87 m/z for PE and PS, respectively. The collision energy optimums for Cer, PE, PC, SM, PI, and PS were 25 eV, 20 eV, 30 eV, 25 eV, 45 eV, and 22 eV, respectively. The corresponding SRM transitions were used to quantify different phospholipid species for each class. Two MRM acquisitions were necessary, due to important differences between phospholipid classes. Data were treated with QqQ Quantitative (vB.05.00) and Qualitative analysis software (vB.04.00).

## Brain proteomic analysis

Protein extracts for each tissue (cerebellum, cortex and hippocampus) and animal were prepared and analyzed via liquid chromatography- mass spectrometry (LC-MS) analysis. Protein extracts were obtained by lysis in RIPA buffer (50mM Tris pH 8, 150 mM NaCl, 1% Triton-X 100, 0.5% sodium deoxycholate, 0.1% sodium dodecylsulfate and 0.25% NP-40) and protein concentration determined via the BCA assay (Pierce-Thermo, San Jose, CA, USA). Peptide digests of 100μg of protein were prepared for each of the tissue lysates using the filter aided sample preparation (FASP) after spiking with recombinant green fluorescent protein (GFP) into each sample at a concentration of 100fmol per 1μg protein extract as previously described [35]. Samples were desalted via C18 reverse phase chromatography and dried. All samples were resuspended in 100μL 0.1% (v/v) formic acid prior to LC-MS analysis.

## LC-MS analysis

One microliter of each sample was injected for label-free, quantitative LC-MS analysis. Mass detection was carried out with a Q-Exactive mass spectrometer (Thermo Fisher Scientific, Bremen, Germany) equipped with an Agilent HPLC system. Chromatographic separation of peptides was accomplished using a Zorbax 300SB-C18 column (3.5μm i.d. x 150mm, particle size 5μm, pore size 100Å, Agilent Technologies, Wilminton, DE). Peptides were loaded onto a Zorbax 300SB-C18 trap cartridge at a flow rate of 2μl per minute for 10 min. After washing with 0.1% formic the peptides were eluted using a 5–60% B gradient for 180 min at a flow rate of 250 nl min$^{-1}$ acid (mobile phase A = 0.1% formic acid; mobile phase B = 0.1% formic acid in acetonitrile). The mass spectrometer was operated in a Top 10 data-dependent mode with automatic switching between MS and MS/MS with HCD fragmentation. Source ionization parameters were as follows: spray voltage, 1.5 kV; capillary temperature, 280° C; and s-lens level, 50.0. Full-scan MS mode ($m/z$ 300–1700) was operated at a resolution of 70 000 with automatic gain control (AGC), target of $1 \times 10^6$ ions and a maximum ion transfer (IT) of 250 milliseconds. Ions selected for MS/MS were subjected to the following parameters: resolution, 17, 500; AGC, $1 \times 10^5$ ions; maximum IT, 100 milliseconds; 1.5 $m/z$ isolation window; normalized collision energy 27.0, and dynamic exclusion, 30 seconds.

## Protein identification and label-free quantification

Raw data was searched against both the SwissProt *Mus musculus* (20,239 sequences) and an in house GFP database using the Proteome Discoverer software (v2.3,

Thermo Fisher, Carlsbad, CA). Trypsin was set as the protease with two missed cleavages and searches were performed with precursor and fragment mass error tolerances set to 10 ppm and 0.02 Da, respectively, where only peptides precursors of +2, +3 and +4 were considered. Peptide variable modifications allowed during the search were: oxidation (M) and deamination (NQ), whereas carbamidomethyl (C) was set as fixed modifications. Label-free relative quantitation analysis was performed across tissue types using the average of the top 3 peptides for each protein where normalization was performed across all samples and all tissues using the intensity of the GFP internal standard. Differentially expressed proteins for NMR relative to mice for each tissue type was determined by applying a Permutation test ($p \leq 0.05$). Raw data is available at: ftp://massive.ucsd.edu/MSV000085798/raw/.

## Brain fatty acid analysis

To measure the totalbrain molecular species derivatized with a methyl ester (FAME), internal standard, glyceryl triheptadecanoate (2 μg), was added to 40 μL of lipid extract. The lipid extract was transmethylated with 1 ml BF3 in methanol (14% solution; Sigma) and 1 ml heptane for 60 min at 80° C and evaporated to dryness. The FAMEs were extracted with heptane/water (2:1). The organic phase was evaporated to dryness and dissolved in 50 μl ethyl acetate. A sample (1 μl) of total FAME was analysed with gas-liquid chromatography (Clarus 600 Perkin Elmer system, with Famewax RESTEK fused silica capillary columns, 30-mm × 0.32-mm i.d., 0.25-μm film thickness). Oven temperature was programmed to increase from 110° C to 220° C at a rate of 2° C/min, and the carrier gas was hydrogen (7.25 psi). Injector and detector temperatures were 225° C and 245° C, respectively.

## Atomic force microscopy

AFM experiments were performed on an Agilent 5500 with closed loop scanners using a liquid cell for imaging of supported lipid bilayers. All experiments were carried out at 20° C. Tapping mode imaging was performed using aluminium coated cantilevers (PPP-NCSTR, Apex Probes, UK) and all images were obtained in PBS buffer. Contact mode images were obtained using contact mode aluminium coated silicon cantilevers (PPP-CONTR, Apex Probes, UK) having nominal spring constants of between 0.02 and 0.77 N m$^{-1}$ and typical tip radius of curvatures of less than 7 nm.

## Aβ preparation

Beta-amyloid (1-42), human (Anaspec) was reconstituted with 1.0% NH$_4$OH and aliquoted before freezing. Before use the aliquot was defrosted and made

up to the desired concentration with PBS buffer. This solution was then vortexed for 2 minutes before being added to the supported lipid bilayer. For all experiments 200 μl of 8 μM Aβ solution was added to the supported bilayer and left for 2 hr. This was removed by gentle pipetting and the bilayer was rinsed gently three times in PBS buffer to remove any free floating Aβ.

**Preparation of supported lipid bilayers**

2-Dipalmitoyl-*sn*-glycero-3-phosphocholine (DOPC) and 1, 2-dioleoyl-*sn*-glycero-3-phosphocholine (DPPC) (Avanti Polar Lipids) were dissolved in chloroform in a 3 to 1 molar ratio and dried under nitrogen. These lipids mixtures were then re-suspended in ultrapure water to a final concentration of 1 mg/ml and intensively vortexed at room temperature. For brain derived lipids the lipids were dried down to form a film and then resuspended in ultrapure water. Uni-lamellar vesicles were formed via ten cycles of freeze-thawing followed by extrusion ten times) through a polycarbonate membrane with pores sizes of 100 nm using a mini-extruder (Avanti Polar Lipids) kept 50° C on a hotplate. 200 μl of solution containing the extruded vesicles was pipetted onto freshly cleaved muscovite mica and this was then placed on a thin metal disk that itself was placed on a hotplate. The hotplate was heated up to 50° C and the sample was annealed for 15 minutes. The sample was then loaded into the AFM liquid cell ready for imaging.

**Breakthrough force measurements**

Indentation measurements were made using contact mode aluminium coated silicon cantilevers (PPP-CONTR, Apex Probes, UK) having nominal spring constants of between 0.02 and 0.77 N m$^{-1}$ and typical tip radius of curvatures of less than 7 nm. The spring constants were calibrated using the equipartition theorem (Thermal K). Actual measured spring constant values were between 0.05 and 0.18 Nm$^{-1}$. Force volume indentation grids of 256 points (16´16) were taken at no less than three different areas across the bilayer. Indentation rate was 1mm/s which was the optimum rate for measuring breakthrough events. Force distance curves were analyzed using a Scanning Probe Image Processor (Image Metrology, Lyngby, Denmark) and in house developed batch analysis code based on the methodology proposed by Li et al [36].

**Statistical analysis**

Data are presented as means ± standard error of the mean (SEM). Analyses were performed using GraphPad Prism 6.0 software (GraphPad, San Diego, CA). Comparisons between groups were performed by the Mann-Whitney test. Statistical significance was set at P < 0.05. The heatmaps were created with the R software (www.r-project.org) with R package, Marray. Ward's algorithm, modified by Murtagh and Legendre, was used as the clustering method.

## CONFLICTS OF INTEREST

These authors declare no conflicts of interest.

## REFERENCES

1. Schuhmacher LN, Husson Z. The naked mole-rat as an animal model in biomedical research: current perspectives. Open Access Animal Physiology. 2015.
https://doi.org/10.2147/OAAP.S50376

2. Ruby JG, Smith M, Buffenstein R. Naked Mole-Rat mortality rates defy gompertzian laws by not increasing with age. Elife. 2018; 7:e31157.
https://doi.org/10.7554/eLife.31157
PMID:29364116

3. Skulachev VP, Holtze S, Vyssokikh MY, Bakeeva LE, Skulachev MV, Markov AV, Hildebrandt TB, Sadovnichii VA. Neoteny, prolongation of youth: from naked mole rats to "naked apes" (humans). Physiol Rev. 2017; 97:699–720.
https://doi.org/10.1152/physrev.00040.2015
PMID:28202600

4. Buffenstein R, Lewis KN, Gibney PA, Narayan V, Grimes KM, Smith M, Lin TD, Brown-Borg HM. Probing pedomorphy and prolonged lifespan in naked mole-rats and dwarf mice. Physiology (Bethesda). 2020; 35:96–111.
https://doi.org/10.1152/physiol.00032.2019
PMID:32024425

5. Buffenstein R. Negligible senescence in the longest living rodent, the naked mole-rat: insights from a successfully aging species. J Comp Physiol B. 2008; 178:439–45.
https://doi.org/10.1007/s00360-007-0237-5
PMID:18180931

6. Edrey YH, Medina DX, Gaczynska M, Osmulski PA, Oddo S, Caccamo A, Buffenstein R. Amyloid beta and the longest-lived rodent: the naked mole-rat as a model for natural protection from Alzheimer's disease. Neurobiol Aging. 2013; 34:2352–60.
https://doi.org/10.1016/j.neurobiolaging.2013.03.032
PMID:23618870

7. Orr ME, Garbarino VR, Salinas A, Buffenstein R. Extended postnatal brain development in the longest-lived rodent: prolonged maintenance of neotenous traits in the naked mole-rat brain. Front Neurosci. 2016; 10:504.
https://doi.org/10.3389/fnins.2016.00504
PMID:27877105

8. van der Kant R, Goldstein LS, Ossenkoppele R. Amyloid-β-independent regulators of tau pathology in Alzheimer disease. Nat Rev Neurosci. 2020; 21:21–35.
https://doi.org/10.1038/s41583-019-0240-3
PMID:31780819

9. Castellani RJ, Plascencia-Villa G, Perry G. The amyloid cascade and Alzheimer's disease therapeutics: theory versus observation. Lab Invest. 2019; 99:958–70.
https://doi.org/10.1038/s41374-019-0231-z
PMID:30760863

10. Rangachari V, Dean DN, Rana P, Vaidya A, Ghosh P. Cause and consequence of Aβ - lipid interactions in Alzheimer disease pathogenesis. Biochim Biophys Acta Biomembr. 2018; S0005-2736:30084–81.
https://doi.org/10.1016/j.bbamem.2018.03.004
PMID:29526709

11. Henry S, Vignaud H, Bobo C, Decossas M, Lambert O, Harte E, Alves ID, Cullin C, Lecomte S. Interaction of Aβ(1-42) amyloids with lipids promotes "off-pathway" oligomerization and membrane damage. Biomacromolecules. 2015; 16:944–50.
https://doi.org/10.1021/bm501837w PMID:25689632

12. Williams TL, Serpell LC. Membrane and surface interactions of Alzheimer's Aβ peptide—insights into the mechanism of cytotoxicity. FEBS J. 2011; 278:3905–17.
https://doi.org/10.1111/j.1742-4658.2011.08228.x
PMID:21722314

13. Bode DC, Baker MD, Viles JH. Ion channel formation by amyloid-β42 oligomers but not amyloid-β40 in cellular membranes. J Biol Chem. 2017; 292:1404–13.
https://doi.org/10.1074/jbc.M116.762526
PMID:27927987

14. Wang C, Shou Y, Pan J, Du Y, Liu C, Wang H. The relationship between cholesterol level and Alzheimer's disease-associated APP proteolysis/aβ metabolism. Nutr Neurosci. 2019; 22:453–63.
https://doi.org/10.1080/1028415X.2017.1416942
PMID:29325505

15. Seghezza S, Diaspro A, Canale C, Dante S. Cholesterol drives Aβ(1-42) interaction with lipid rafts in model membranes. Langmuir. 2014; 30:13934–41.
https://doi.org/10.1021/la502966m PMID:25360827

16. Habchi J, Chia S, Galvagnion C, Michaels TC, Bellaiche MM, Ruggeri FS, Sanguanini M, Idini I, Kumita JR, Sparr E, Linse S, Dobson CM, Knowles TP, Vendruscolo M. Cholesterol catalyses Aβ42 aggregation through a heterogeneous nucleation pathway in the presence of lipid membranes. Nat Chem. 2018; 10:673–83.
https://doi.org/10.1038/s41557-018-0031-x
PMID:29736006

17. Hulbert AJ. On the importance of fatty acid composition of membranes for aging. J Theor Biol. 2005; 234:277–88.
https://doi.org/10.1016/j.jtbi.2004.11.024
PMID:15757684

18. Hulbert AJ, Faulks SC, Buffenstein R. Oxidation-resistant membrane phospholipids can explain longevity differences among the longest-living rodents and similarly-sized mice. J Gerontol A Biol Sci Med Sci. 2006; 61:1009–18.
https://doi.org/10.1093/gerona/61.10.1009
PMID:17077193

19. Mitchell TW, Buffenstein R, Hulbert AJ. Membrane phospholipid composition may contribute to exceptional longevity of the naked mole-rat (Heterocephalus glaber): a comparative study using shotgun lipidomics. Exp Gerontol. 2007; 42:1053–62.
https://doi.org/10.1016/j.exger.2007.09.004
PMID:18029129

20. Braverman NE, Moser AB. Functions of plasmalogen lipids in health and disease. Biochim Biophys Acta. 2012; 1822:1442–52.
https://doi.org/10.1016/j.bbadis.2012.05.008
PMID:22627108

21. Gorgas K, Teigler A, Komljenovic D, Just WW. The ether lipid-deficient mouse: tracking down plasmalogen functions. Biochim Biophys Acta. 2006; 1763:1511–26.
https://doi.org/10.1016/j.bbamcr.2006.08.038
PMID:17027098

22. Azouz M, Cullin C, Lecomte S, Lafleur M. Membrane domain modulation of Aβ$_{1-42}$ oligomer interactions with supported lipid bilayers: an atomic force microscopy investigation. Nanoscale. 2019; 11:20857–67.
https://doi.org/10.1039/c9nr06361g
PMID:31657431

23. Et-Thakafy O, Guyomarc'h F, Lopez C. Young modulus of supported lipid membranes containing milk sphingomyelin in the gel, fluid or liquid-ordered phase, determined using AFM force spectroscopy. Biochim Biophys Acta Biomembr. 2019; 1861:1523–32.
https://doi.org/10.1016/j.bbamem.2019.07.005
PMID:31295476

24. Pettegrew JW, Panchalingam K, Hamilton RL, McClure RJ. Brain membrane phospholipid alterations in Alzheimer's disease. Neurochem Res. 2001; 26:771–82.
https://doi.org/10.1023/a:1011603916962
PMID:11565608

25. Bhatia T, Cornelius F, Ipsen JH. Exploring the raft-hypothesis by probing planar bilayer patches of free-standing giant vesicles at nanoscale resolution, with and without Na,K-ATPase. Biochim Biophys Acta. 2016; 1858:3041–49.
https://doi.org/10.1016/j.bbamem.2016.09.001
PMID:27616046

26. Garcia-Manyes S, Sanz F. Nanomechanics of lipid bilayers by force spectroscopy with AFM: a perspective. Biochim Biophys Acta. 2010; 1798:741–49.
https://doi.org/10.1016/j.bbamem.2009.12.019
PMID:20044974

27. Bianchi F, Pereno V, George JH, Thompson MS, Ye H. Membrane mechanical properties regulate the effect of strain on spontaneous electrophysiology in human iPSC-derived neurons. Neuroscience. 2019; 404:165–74.
https://doi.org/10.1016/j.neuroscience.2019.02.014
PMID:30817953

28. Filippov A, Orädd G, Lindblom G. Sphingomyelin structure influences the lateral diffusion and raft formation in lipid bilayers. Biophys J. 2006; 90:2086–92.
https://doi.org/10.1529/biophysj.105.075150
PMID:16387761

29. Uttara B, Singh AV, Zamboni P, Mahajan RT. Oxidative stress and neurodegenerative diseases: a review of upstream and downstream antioxidant therapeutic options. Curr Neuropharmacol. 2009; 7:65–74.
https://doi.org/10.2174/157015909787602823
PMID:19721819

30. Schaich KM, Xie J, Bogusz BA. Thinking outside the classical chain reaction box of lipid oxidation: Evidence for alternate pathways and the importance of epoxides. Lipid Technology. 2017; 29:91–96.
https://doi.org/10.1002/lite.201700025

31. Kivipelto M, Solomon A. Cholesterol as a risk factor for Alzheimer's disease - epidemiological evidence. Acta Neurol Scand Suppl. 2006; 185:50–57.
https://doi.org/10.1111/j.1600-0404.2006.00685.x
PMID:16866911

32. Mari SA, Wegmann S, Tepper K, Hyman BT, Mandelkow EM, Mandelkow E, Müller DJ. Reversible cation-selective attachment and self-assembly of human Tau on supported brain lipid membranes. Nano Lett. 2018; 18:3271–81.
https://doi.org/10.1021/acs.nanolett.8b01085
PMID:29644863

33. Browe BM, Olsen AR, Ramirez C, Rickman RH, Smith ES, Park TJ. The naked mole-rat has a functional purinergic pain pathway despite having a non-functional peptidergic pain pathway. Neurobiol Pain. 2020; 8:100047.
https://doi.org/10.1016/j.ynpai.2020.100047
PMID:32478202

34. Petković M, Vocks A, Müller M, Schiller J, Arnhold J. Comparison of different procedures for the lipid extraction from HL-60 cells: a MALDI-TOF mass spectrometric study. Z Naturforsch C J Biosci. 2005; 60:143–51.
https://doi.org/10.1515/znc-2005-1-226
PMID:15787260

35. Pergande MR, Nguyen TT, Haney-Ball C, Davidson CD, Cologna SM. Quantitative, label-free proteomics in the symptomatic niemann-pick, type C1 mouse model using standard flow liquid chromatography and thermal focusing electrospray ionization. Proteomics. 2019; 19:e1800432.
https://doi.org/10.1002/pmic.201800432
PMID:30888112

36. Li JK, Sullan RM, Zou S. Atomic force microscopy force mapping in the study of supported lipid bilayers. Langmuir. 2011; 27:1308–13.
https://doi.org/10.1021/la103927a
PMID:21090659

# SUPPLEMENTARY MATERIALS

## Supplementary Methods

### Production of naked mole-rat amyloid beta

The single point mutation (His13Arg) was introduced to the pET-Sac vector containing a gene encoding for wild type, human Aβ(M1–42) using a QuikChange Site Directed Mutagenesis kit (Agilent UK Ltd., Cheshire, UK) and following the manufacturer's protocol. The primers were: Forward-5'-GGTTACGAAGTTCGC CACCAGAAGCTGG-3' and Reverse - 5'-CCAG CTTCTGGTGGCGAACTTCGTAACC-3'. Plasmid sequences were confirmed by DNA sequencing (Dept. of Biochemistry, University of Cambridge, UK). The recombinant Naked Mole-Rat Aβ(M1-42) peptide (MDAEFRHDSGY EVRHQKLVFFAEDVGSNKGA IIGLMVGGVV IA), here called NMR amyloid beta, was expressed in the E. coli BL21 Gold (DE3) strain (Stratagene, CA, U.S.A.) and purified as described previously with slight modifications[1]. Briefly, the purification procedure involved sonication of E. coli cells, dissolution of inclusion bodies in 8 M urea, and ion exchange in batch mode on diethylaminoethyl cellulose resin followed by lyophylisation. The lyophilised fractions were further purified using Superdex 75 HR 26/60 column (GE Healthcare, Buckinghamshire, U.K.) and eluates were analysed by SDS-PAGE using 4-12% Bis-Tris NuPAGE gels and MES buffer (Thermofisher, Paisley, UK) for the presence of the desired protein product. The fractions containing the recombinant protein were combined, frozen using liquid nitrogen, and lyophilised again. The mass of the NMR amyloid beta was confirmed by mass spectrometry (Department of Chemistry, University of Cambridge, UK) (calculated mass: 4664.3 Da; observed mass: $4663.4 \pm 0.8$ Da).

### Thioflavin T (ThT) kinetic assay

A sample of lyophilised naked mole-rat amyloid beta was dissolved in 1 ml GdnHCl (6 M, pH 8) and incubated on ice (1.5-2 hr). SEC was performed on the NMR Aβ42 using a Superdex 75 10/300 GL column (GE Healthcare, Amersham, UK). The buffer used for elution was a pH 8 sodium phosphate buffer (25mM $Na_2PO_4$, 0.2mM EDTA, pH 8) (flow rate 0.7 ml/min). Solutions containing monomer were collected and monomer concentrations were determined by the UV absorbance of the solution ($\varepsilon_{280\ nm}$ =1490 $M^{-1}cm^{-1}$). The monomer obtained in this way was diluted with buffer to the desired concentration and supplemented with 20 μM Thioflavin T (ThT) from a 1 mM stock. All samples were prepared in low binding eppendorf tubes on ice using careful pipetting to avoid introduction of air bubbles. Each sample was then pipetted into multiple wells of a 96-well half-area, low-binding, clear bottom and PEG coated plate (Corning 3881), to give 80 μL per well. Kinetics assays were initiated by placing the 96-well plate at 37 °C under quiescent conditions in a plate reader (Fluostar Omega, BMGLabtech, Offenburg, Germany). The ThT fluorescence was measured through the bottom of the plate with a 440 nm excitation filter and a 480 nm emission filter. The ThT fluorescence was followed for three repeats of each sample.

### Transmission electron microscopy

5μl of NMR and human Aβ42 aggregate solutions were applied to carbon-coated copper grids, stained with 2% (w/v) uranyl acetate and washed twice with 5 μl MilliQ water. The grids were then imaged with a Thermo Scientific Talos F200X G2 200 kV FEG Scanning Transmission Electron Microscope (Department of Chemistry, University of Cambridge).

## Supplementary Reference

1. Hellstrand E, Boland B, Walsh DM, Linse S. Amyloid β-protein aggregation produces highly reproducible kinetic data and occurs by a two-phase process. ACS Chem Neurosci. 2010; 1:13–8.
   https://doi.org/10.1021/cn900015v
   PMID:22778803

# Supplementary Figures
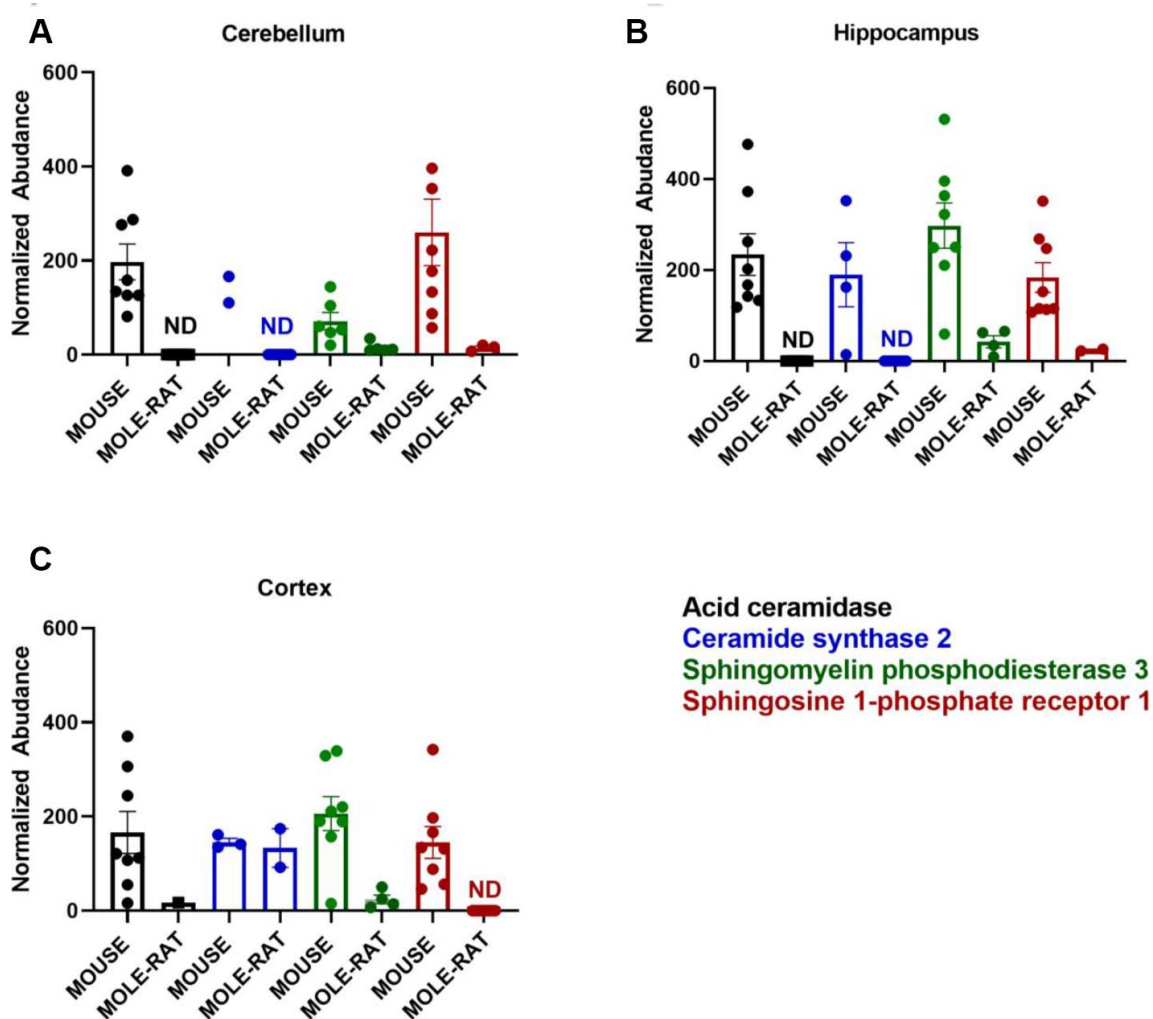


**Supplementary Figure 1. Normalized abundance of proteins related to lipid metabolism and function in different brain regions in mouse and naked mole-rat.** The normalized abundance of acid ceramidase, ceramide synthase 2, sphingomyelin phosphodiesterase 3 and sphingosine 1-phosphate receptor 1 are provided for cerebellum (**A**), hippocampus (**B**) and cortex (**C**) for mouse and naked mole-rat.
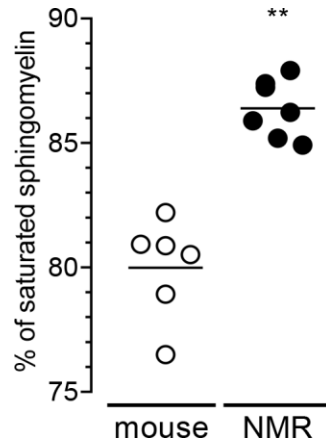
**Supplementary Figure 2. Percentage of saturated sphingomyelin. Lipids were extracted from the brains of 7 naked mole-rats and 6 mice (2 independent experiments).** % of saturated sphingomyelin in lipid extract from mouse (white circle) or naked mole-rat (black circle) brains. Data are represented as scatter dot plot with the mean. Statistical analysis was performed using the Mann-Whitney test. **p<0.01, significantly different from mouse group.
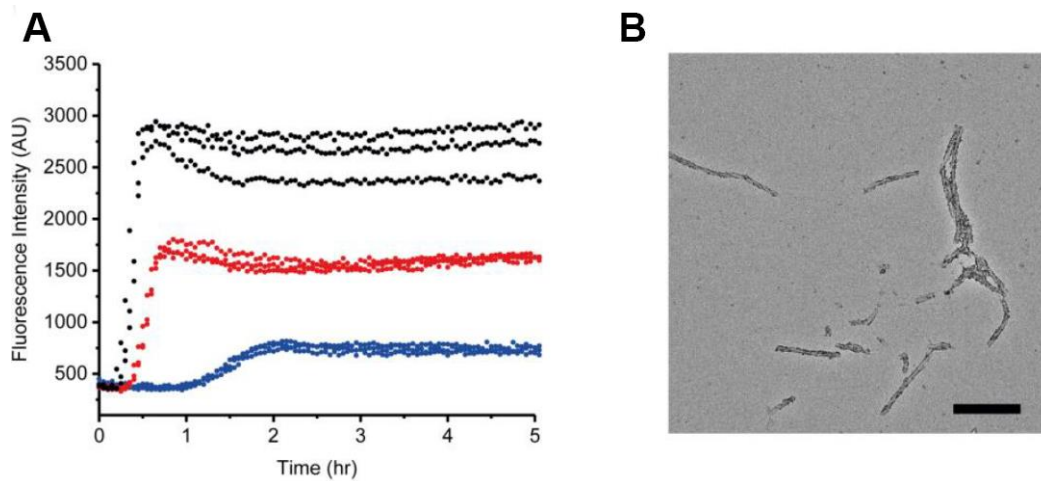


**Supplementary Figure 3.** (**A**) ThT kinetics traces for 1 µM (blue), 3 µM (red) and 5 µM (black) naked mole-rat amyloid beta shown in triplicate (pH 8, 37°C, quiescent conditions). Representative of two independent experiments. (**B**) TEM analysis of endpoint fibrils formed from kinetics assay (scale bar = 200 nm). Results indicative of a single batch of naked mole-rat amyloid beta.
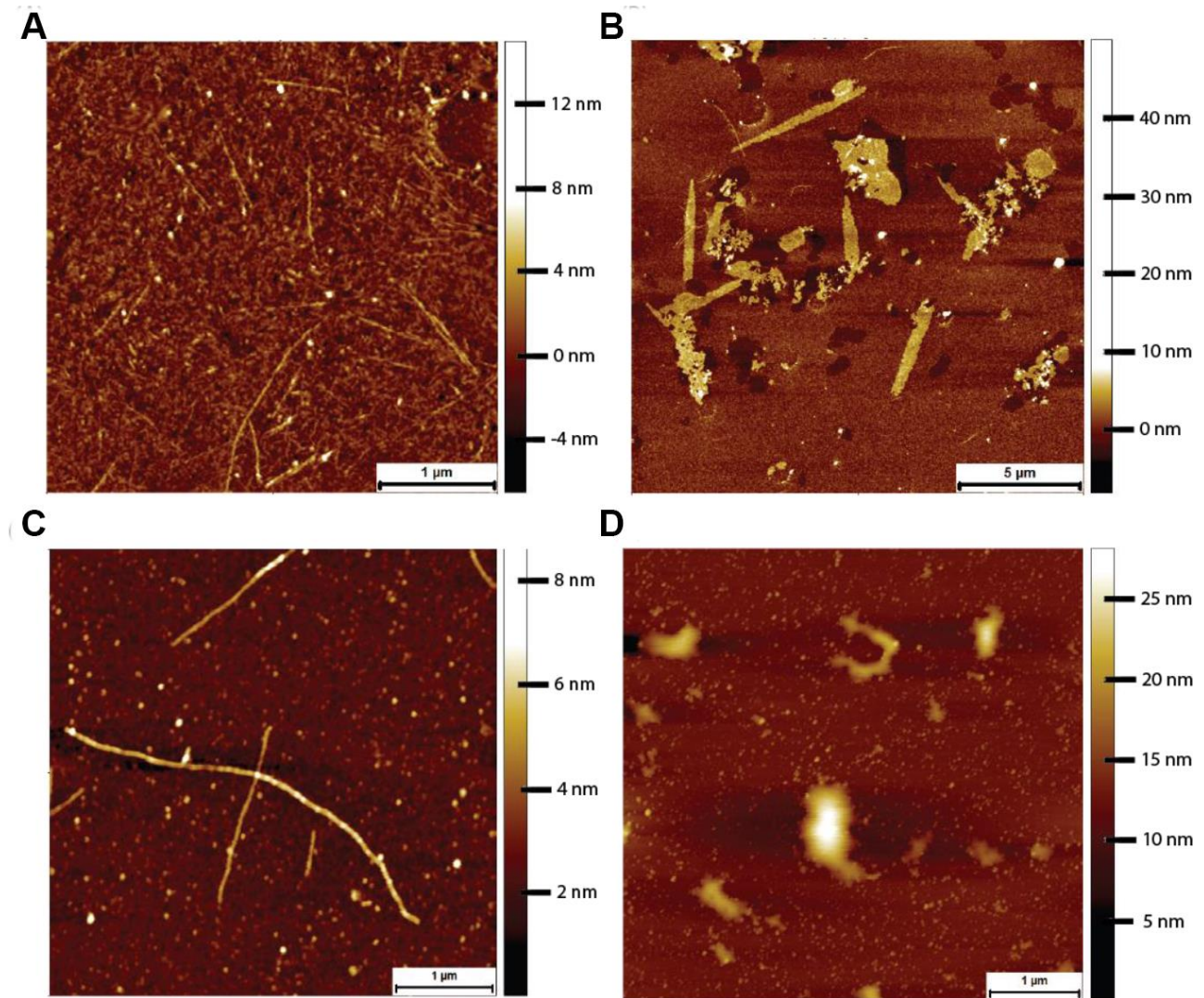
**Supplementary Figure 4. Amyloid beta peptide adsorbed (air dried) onto mica at a concentration of 8 µM.** (**A**) Synthetic human amyloid beta readily forms fibres. (**B**) Higher order structures of the human amyloid beta. These are well organised, and the constituent fibres are resolvable. (**C**) Recombinantly expressed naked mole-rat amyloid beta also forms fibres. (**D**) Less well-defined higher order structures are formed by naked mole-rat amyloid beta.
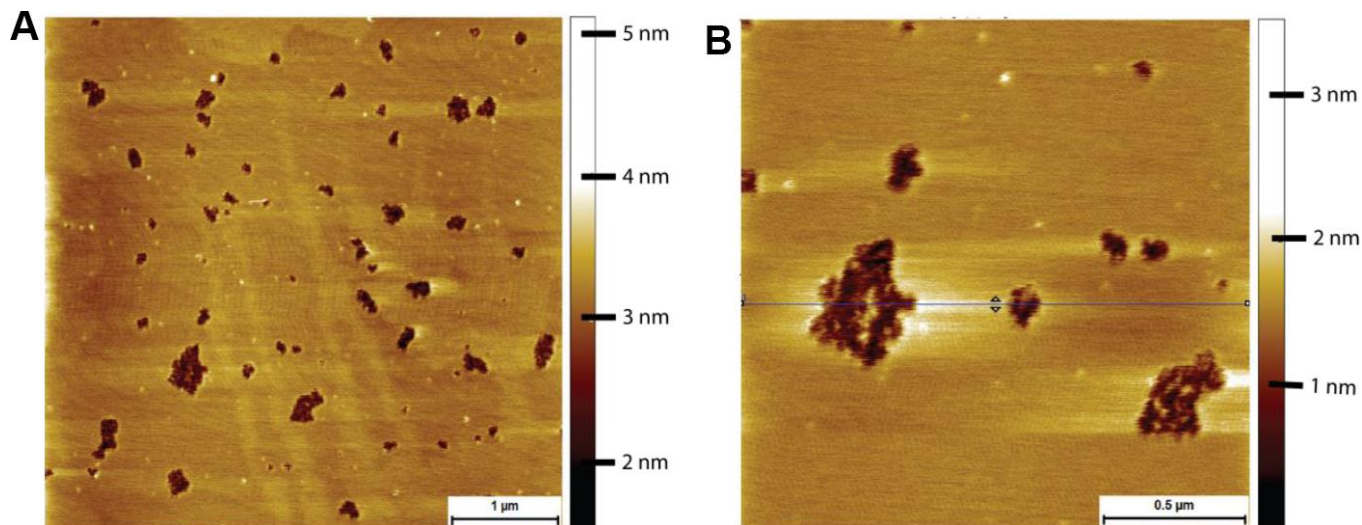
**Supplementary Figure 5. AFM tapping mode images (in PBS) of mouse brain tissue derived supported lipid bilayers exposed to 8 μM of naked mole-rat amyloid beta for 2 hr.** (**A**) Supported bilayer made from mouse brain derived lipids exhibiting naked mole-rat amyloid beta induced holes. (**B**) High resolution tapping mode image of naked mole-rat amyloid beta induced holes in mouse brain lipid derived bilayers. Holes do not penetrate bilayer.
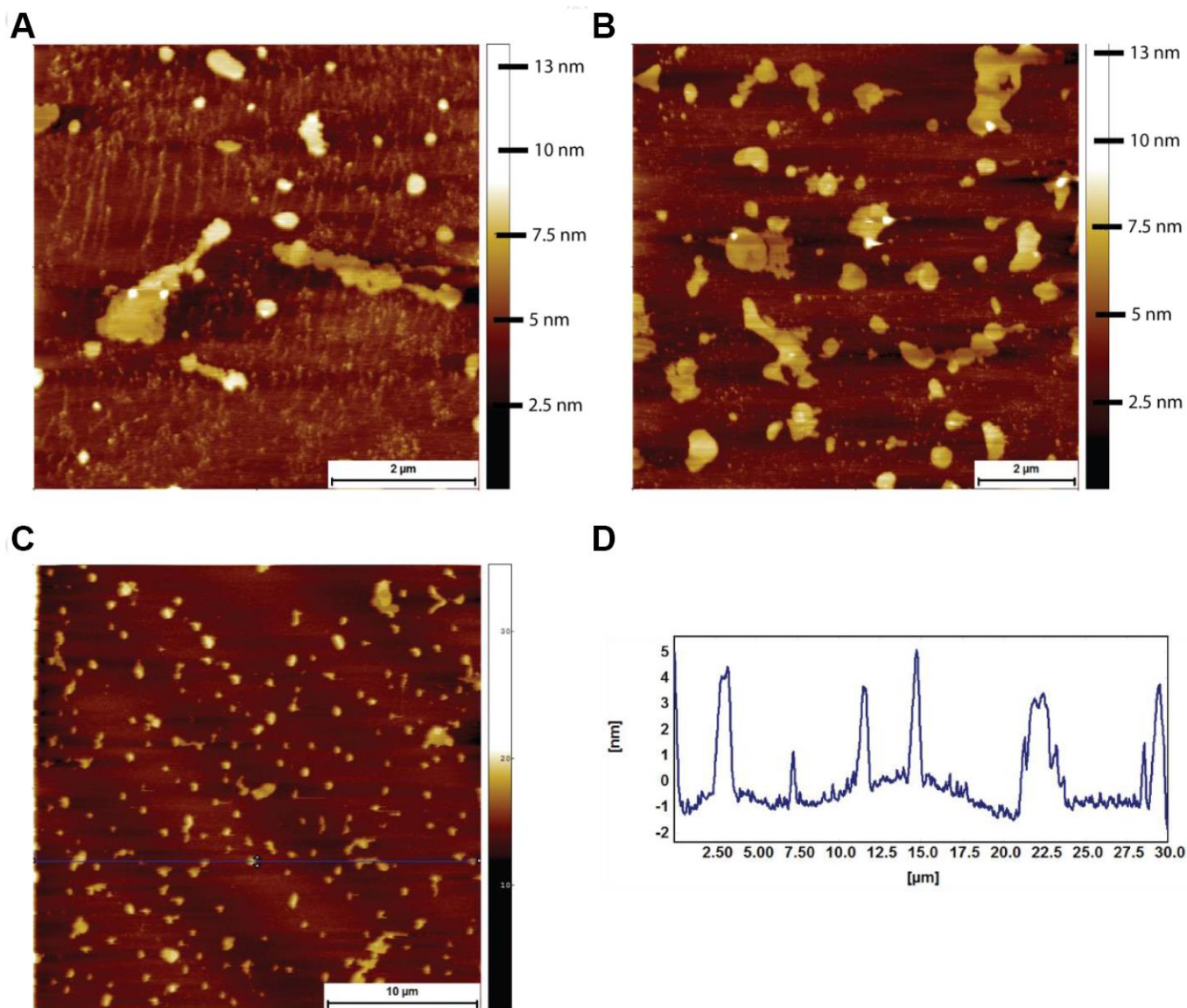
**Supplementary Figure 6. AFM tapping mode images (in PBS) of naked mole-rat brain derived lipid bilayers exposed to 8 μM of naked mole-rat amyloid beta for 2 hr.** (**A** and **B**) The bilayer is reduced to fragments of membrane, the height of fragments consistent with bilayer thickness. (**C**) Large scale topographic image showing the scale of the damage. (**D**) A height profile corresponding to the blue horizontal line in (**C**), confirming the height of fragments to be of bilayer thickness of 5-6 nm.

# Supplementary Tables

**Supplementary Table 1. percentage of phosphatidylcholine from mouse and naked mole rat brains.**

| Lipid number | % of total phosphatidylcholine | | P value |
| --- | --- | --- | --- |
| | Naked mole rat | Mouse | |
| PC 28:0 | $0.87 \pm 0.12$ | $0.021 \pm 0.003$ | 0.0012 |
| PC 30:0 | $8.80 \pm 0.78$ | $0.91 \pm 0.10$ | 0.0012 |
| PC 30:1 | $2.70 \pm 1.04$ | $0.59 \pm 0.26$ | 0.2343 |
| PC 32:0 | $22.04 \pm 0.55$ | $32.98 \pm 0.58$ | 0.0012 |
| PC 32:1 | $5.00 \pm 0.86$ | $1.08 \pm 0.24$ | 0.0012 |
| PC 32:2 | $0.14 \pm 0.007$ | $0.008 \pm 0.0007$ | 0.0012 |
| PC 34:0 | $2.90 \pm 0.09$ | $3.41 \pm 0.10$ | 0.0082 |
| PC 34:1 | $18.45 \pm 0.61$ | $17.67 \pm 0.44$ | 0.4452 |
| PC 34:2 | $1.50 \pm 0.10$ | $0.66 \pm 0.02$ | 0.0012 |
| PC 34:3 | $0.15 \pm 0.01$ | $0.02 \pm 0.001$ | 0.0012 |
| PC 36:1 | $4.19 \pm 0.09$ | $7.68 \pm 0.08$ | 0.0012 |
| PC 36:2 | $2.57 \pm 0.19$ | $2.98 \pm 0.17$ | 0.1014 |
| PC 36:3 | $1.51 \pm 0.06$ | $1.20 \pm 0.03$ | 0.0012 |
| PC 36:4 | $6.47 \pm 0.12$ | $5.69 \pm 0.08$ | 0.0012 |
| PC 38:2 | $0.21 \pm 0.02$ | $0.50 \pm 0.01$ | 0.0012 |
| PC 38:3 | $1.21 \pm 0.02$ | $1.07 \pm 0.01$ | 0.0012 |
| PC 38:4 | $7.83 \pm 0.35$ | $6.93 \pm 0.25$ | 0.1375 |
| PC 38:5 | $3.70 \pm 0.10$ | $2.43 \pm 0.33$ | 0.0012 |
| PC 38:6 | $3.98 \pm 0.05$ | $5.68 \pm 0.20$ | 0.0012 |
| PC 40:3 | $0.097 \pm 0.002$ | $0.08 \pm 0.002$ | 0.0140 |
| PC 40:6 | $5.64 \pm 0.07$ | $8.35 \pm 0.26$ | 0.0012 |

Values are expressed as mean ± SEM; Statistical analysis was performed using Mann-Whitney test.

**Supplementary Table 2. percentage of phosphatidylethanolamine from mouse and naked mole rat brains.**

| Lipid number | % of total phosphatidylethanolamine | | P value |
| --- | --- | --- | --- |
| | Naked mole rat | Mouse | |
| PE 32:0 | $0.50 \pm 0.01$ | $0.39 \pm 0.03$ | 0.0140 |
| PE 32:1 | $0.56 \pm 0.07$ | $0.18 \pm 0.02$ | 0.0012 |
| PE 32:2 | $0.040 \pm 0.004$ | $0.007 \pm 0.001$ | 0.0012 |
| PE 34:0 | $8.88 \pm 1.12$ | $8.39 \pm 1.02$ | 0.2343 |
| PE 34:1 | $1.04 \pm 0.15$ | $0.57 \pm 0.06$ | 0.0221 |
| PE 36:1 | $8.46 \pm 0.64$ | $14.50 \pm 0.40$ | 0.0012 |
| PE 36:2 | $4.71 \pm 0.76$ | $7.32 \pm 0.88$ | 0.0350 |
| PE 36:3 | $1.77 \pm 0.11$ | $1.31 \pm 0.16$ | 0.1014 |
| PE 36:4 | $1.79 \pm 0.09$ | $1.42 \pm 0.07$ | 0.0140 |
| PE 38:2 | $1.83 \pm 0.17$ | $1.90 \pm 0.10$ | 0.9452 |
| PE 38:3 | $13.78 \pm 2.55$ | $8.26 \pm 1.77$ | 0.1014 |
| PE 38:4 | $16.55 \pm 0.22$ | $11.46 \pm 0.22$ | 0.0012 |
| PE 38:5 | $3.81 \pm 0.43$ | $5.25 \pm 0.54$ | 0.1014 |
| PE 38:6 | $4.40 \pm 0.24$ | $4.77 \pm 0.53$ | 0.9452 |
| PE 40:3 | $3.57 \pm 0.65$ | $1.96 \pm 0.38$ | 0.1014 |
| PE 40:5 | $12.14 \pm 1.35$ | $13.0\& \pm 2.26$ | 0.7308 |
| PE 40:6 | $14.60 \pm 1.66$ | $17.85 \pm 1.80$ | 0.1014 |
| PE 40:7 | $1.55 \pm 0.30$ | $1.42 \pm 0.26$ | 0.2343 |

Values are expressed as mean ± SEM; Statistical analysis was performed using Mann-Whitney test.

**Supplementary Table 3. percentage of phosphatidylinositol from mouse and naked mole rat brains.**

| Lipid number | % of total phosphatidylinositol | | |
|---|---|---|---|
| | Naked mole rat | Mouse | P value |
| PI 32:1 | 0.19 ± 0.02 | 0.147 ± 0.008 | 0.1014 |
| PI 34:1 | 1.40 ± 0.19 | 2.08 ± 0.06 | 0.0350 |
| PI 34:2 | 0.39 ± 0.07 | 0.38 ± 0.02 | 0.4452 |
| PI 36:0 | 0.24 ± 0.02 | 0.66 ± 0.04 | 0.0012 |
| PI 36:1 | 0.81 ± 0.09 | 2.10 ± 0.07 | 0.0012 |
| PI 36:2 | 0.67 ± 0.08 | 0.90 ± 0.02 | 0.1807 |
| PI 36:3 | 2.36 ± 0.11 | 2.58 ± 0.20 | 0.4452 |
| PI 38:1 | 0.10 ± 0.01 | 0.285 ± 0.008 | 0.0012 |
| PI 38:2 | 1.02 ± 0.04 | 1.04 ± 0.05 | 0.7308 |
| PI 38:3 | 18.49 ± 1.08 | 17.34 ± 1.04 | 0.1375 |
| PI 38:4 | 55.34 ± 0.38 | 52.74 ± 0.27 | 0.0012 |
| PI 38:5 | 16.58 ± 0.87 | 14.51 ± 0.99 | 0.2343 |
| PI 40:2 | 0.026 ± 0.001 | 0.032 ± 0.008 | 0.9452 |
| PI 40:3 | 0.118 ± 0.003 | 0.159 ± 0.007 | 0.0012 |
| PI 40:4 | 0.377 ± 0.009 | 0.51 ± 0.01 | 0.0012 |
| PI 40:5 | 0.73 ± 0.05 | 1.39 ± 0.05 | 0.0012 |
| PI 40:6 | 1.16 ± 0.15 | 3.13 ± 0.15 | 0.0012 |

Values are expressed as mean ± SEM; Statistical analysis was performed using Mann-Whitney test.

**Supplementary Table 4. percentage of phosphatidylserine from mouse and naked mole rat brains.**

| Lipid number | % of total phosphatidylserine | | |
|---|---|---|---|
| | Naked mole rat | Mouse | P value |
| PS 32:0 | 0.027 ± 0.001 | 0.011 ± 0.001 | 0.0023 |
| PS 34:0 | 0.57 ± 0.02 | 0.48 ± 0.01 | 0.0047 |
| PS 34:1 | 2.37 ± 0.12 | 1.58 ± 0.02 | 0.0012 |
| PS 34:2 | 0.19 ± 0.01 | 0.091 ± 0.002 | 0.0012 |
| PS 36:0 | 2.03 ± 0.16 | 3.27 ± 0.08 | 0.0012 |
| PS 36:1 | 6.66 ± 0.36 | 12.22 ± 0.37 | 0.0012 |
| PS 36:2 | 3.32 ± 0.14 | 4.88 ± 0.16 | 0.0012 |
| PS 36:3 | 0.345 ± 0.007 | 0.188 ± 0.003 | 0.0012 |
| PS 38:2 | 0.74 ± 0.03 | 0.86 ± 0.04 | 0.0350 |
| PS 38:3 | 2.57 ± 0.10 | 1.84 ± 0.06 | 0.0023 |
| PS 38:4 | 5.29 ± 0.07 | 3.71 ± 0.13 | 0.0012 |
| PS 38:6 | 0.38 ± 0.04 | 0.61 ± 0.06 | 0.0221 |
| PS 40:5 | 23.33 ± 0.43 | 18.02 ± 0.21 | 0.0012 |
| PS 40:6 | 51.91 ± 0.43 | 52.01 ± 0.32 | 0.5338 |
| PS 42:6 | 0.263 ± 0.009 | 0.23 ± 0.01 | 0.1807 |

Values are expressed as mean ± SEM; Statistical analysis was performed using Mann-Whitney test.

**Supplementary Table 5. percentage of sphingomyelin from mouse and naked mole rat brains.**

| Lipid number | % of total sphingomyelin | | P value |
|---|---|---|---|
| | Naked mole rat | Mouse | |
| SM 18:1/14:0 | 1.95 ± 0.07 | 0.113 ± 0.008 | 0.0012 |
| SM 18:1/16:0 | 20.05 ± 0.95 | 4.16 ± 0.18 | 0.0012 |
| SM 18:1/16:1 | 0.46 ± 0.05 | 0.131 ± 0.009 | 0.0012 |
| SM 18:1/18:0 | 58.86 ± 0.68 | 68.62 ± 1.05 | 0.0012 |
| SM 18:1/18:1 | 5.46 ± 0.54 | 5.79 ± 0.39 | 0.9452 |
| SM 18:1/20:0 | 1.61 ± 0.14 | 2.53 ± 0.31 | 0.0734 |
| SM 18:1/20:1 | 0.150 ± 0.009 | 0.35 ± 0.02 | 0.0012 |
| SM 18:1/22:0 | 1.08 ± 0.18 | 1.54 ± 0.16 | 0.1014 |
| SM 18:1/22:1 | 0.56 ± 0.05 | 0.83 ± 0.13 | 0.2949 |
| SM 18:1/24:0 | 2.83 ± 0.33 | 3.03 ± 0.11 | 0.7308 |
| SM 18:1/24:1 | 6.98 ± 0.77 | 12.90 ± 0.52 | 0.0012 |

Values are expressed as mean ± SEM; Statistical analysis was performed using Mann-Whitney test.

**Supplementary Table 6. percentage of ceramide from mouse and naked mole rat brains.**

| Lipid number | % of total ceramide | | P value |
|---|---|---|---|
| | Naked mole rat | Mouse | |
| Cer d18:1/16:0 | 12.39 ± 0.66 | 1.99 ± 0.06 | 0.0012 |
| Cer d18:1/16:1 | 0.087 ± 0.003 | 0.018 ± 0.001 | 0.0012 |
| Cer d18:1/18:0 | 77.92 ± 0.38 | 85.18 ± 1.70 | 0.0012 |
| Cer d18:1/18:1 | 1.15 ± 0.07 | 0.91 ± 0.09 | 0.1375 |
| Cer d18:1/20:0 | 0.76 ± 0.03 | 3.40 ± 0.08 | 0.0012 |
| Cer d18:1/22:0 | 1.11 ± 0.06 | 1.35 ± 0.10 | 0.1014 |
| Cer d18:1/24:0 | 3.06 ± 0.44 | 3.12 ± 0.71 | >0.9999 |
| Cer d18:1/24:1 | 3.45 ± 0.47 | 3.97 ± 0.99 | 0.8357 |
| Cer d18:1/26:0 | 0.033 ± 0.008 | 0.023 ± 0.008 | 0.2343 |
| Cer d18:1/26:1 | 0.038 ± 0.007 | 0.022 ± 0.006 | 0.1014 |

Values are expressed as mean ± SEM; Statistical analysis was performed using Mann-Whitney test.

**Supplementary Table 7. Relative concentration of fatty acid from mouse and naked mole rat brains.**

| Common name | Lipid number | Relative concentration per g of tissue | | P value |
|---|---|---|---|---|
| | | Mouse | Naked mole rat | |
| Myristic acid | C14:0 | 0.84 ± 0.08 | 2.53 ± 0.19 | 0.0025 |
| Palmitic acid | C16:0 | 0.73 ± 0.02 | 1.14 ± 0.05 | 0.0012 |
| Stearic acid | C18:0 | 670.90 ± 69.27 | 526.00 ± 33.00 | 0.1375 |
| Hypogeic acid | C16:1 n-9 | 3.03 ± 0.50 | 17.90 ± 2.14 | 0.0012 |
| Palmitoleic acid | C16:1 n-7 | 8.62 ± 1.25 | 11.00 ± 1.13 | 0.2774 |
| Elaidic acid | C18:1 n-9 | 540.60 ± 59.06 | 425.70 ± 21.36 | 0.1807 |
| Vaccenic acid | C18:1 n-7 | 117.50 ± 13.06 | 110.20 ± 5.10 | 0.6282 |
| Gondoic acid | C20:1 n-9 | 75.29 ± 11.01 | 35.49 ± 6.50 | 0.0140 |
| Linoleic acid | C18:2 n-6 | 20.48 ± 2.86 | 22.66 ± 2.13 | 0.8357 |
| α-Linolenic acid | C18:3 n-3 | 0.87 ± 0.14 | 0.87 ± 0.14 | 0.9452 |
| Eicosadienoic acid | C20:2 n-6 | 8.77 ± 1.09 | 9.39 ± 1.03 | 0.7308 |
| Dihomo-γ-linolenic acid | C20:3 n-6 | 19.39 ± 2.25 | 21.26 ± 1.79 | 0.5589 |
| Arachidonic acid | C20:4 n-6 | 353.40 ± 42.06 | 360.10 ± 29.88 | 0.8357 |
| Eicosapentaenoic acid | C20:5 n-3 | 1.11 ± 0.15 | 5.40 ± 0.89 | 0.0012 |
| Docosatrienoic acid | C22:3 n-3 | 7.81 ± 1.17 | 24.20 ± 3.36 | 0.0023 |
| Adrenic acid | C22:4 n-6 | 89.30 ± 11.63 | 93.05 ± 10.27 | 0.9999 |
| Docosapentaenoic acid | C22:5 n-3 | 11.77 ± 2.09 | 38.43 ± 3.11 | 0.0012 |
| Docosahexaenoic acid | C22:6 n-3 | 660.00 ± 88.74 | 382.30 ± 1.67 | 0.0221 |

Values are expressed as mean ± SEM; Statistical analysis was performed using Mann-Whitney test.